



1 **Measurement report: Atmospheric nitrate radical chemistry in the**
2 **South China Sea influenced by the urban outflow of the Pearl River**
3 **Delta**

4 Jie Wang^{1,2}, Haichao Wang^{1,2*}, Yee Jun Tham^{3,4*}, Lili Ming⁵, Zelong Zheng¹, Guizhen
5 Fang³, Cuizhi Sun^{1,2}, Zhenhao Ling^{1,2}, Jun Zhao^{1,2}, Shaojia Fan^{1,2}

6 ¹ School of Atmospheric Sciences, Sun Yat-sen University, and Southern Marine Science
7 and Engineering Guangdong Laboratory (Zhuhai), Zhuhai, 519082, China

8 ² Guangdong Provincial Observation and Research Station for Climate Environment and
9 Air Quality Change in the Pearl River Estuary, Key Laboratory of Tropical Atmosphere-
10 Ocean System (Sun Yat-sen University), Ministry of Education, Zhuhai, 519082, China

11 ³ School of Marine Sciences, Sun Yat-sen University, Zhuhai 519082, China.

12 ⁴ Pearl River Estuary Marine Ecosystem Research Station, Ministry of Education, Zhuhai,
13 519082, China.

14 ⁵ Technical Center of Gongbei Customs District of China, Zhuhai, 519000, China.

15

16 *Correspondence to:* Haichao Wang (wanghch27@mail.sysu.edu.cn); Yee Jun Tham
17 (thamyj@mail.sysu.edu.cn)

18

19 **Abstract.** Nitrate radical (NO₃) is a critical nocturnal atmospheric oxidant in the
20 troposphere, which widely affects the fate of air pollutants and regulates air quality. Many
21 previous works have reported the chemistry of NO₃ in inland regions of China, while less
22 study targets marine regions. Here, we present a field measurement of the NO₃ reservoir,
23 dinitrogen pentoxide (N₂O₅), and related species at a typical marine site (Da Wan Shan
24 Island) located in the South China Sea in the winter of 2021. Two patterns of air masses
25 were captured during the campaign, including the dominant airmass from inland China
26 (IAM) with a percentage of ~84%, and the airmass from eastern coastal areas (CAM) with
27 ~16%. During the IAM period, the NO₃ production rate reached 1.6 ± 0.9 ppbv h⁻¹ due to
28 the transportation of the polluted urban plume with high NO_x and O₃. While the average
29 nocturnal N₂O₅ and the calculated NO₃ mixing ratio were 119.5 ± 128.6 pptv and $9.9 \pm$
30 12.5 pptv, respectively, and the steady state lifetime of NO₃ was 0.5 ± 0.7 min on average,
31 indicating intensive nighttime chemistry and rapid NO₃ loss at this site. By examining the
32 reaction of NO₃ with volatile organic compounds (VOCs) and N₂O₅ heterogeneous
33 hydrolysis, we revealed that these two reaction pathways were not responsible for the NO₃
34 loss (<20%), since the NO₃ reactivity ($k(\text{NO}_3)$) towards VOCs was small (5.2×10^{-3} s⁻¹)

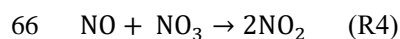
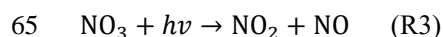
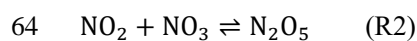
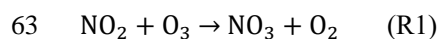


35 and the aerosol loading was low. Instead, NO was proposed to significantly contribute to
36 nocturnal NO₃ loss at this site, despite the nocturnal NO concentration always at sub-ppbv
37 level and near the instrument detection limit. It might be from the local soil emission. We
38 infer that the nocturnal chemical NO₃ reactions would be largely enhanced once without
39 NO emission in the open ocean after the air mass passes through this site, thus highlighting
40 the strong influences of the urban outflow to the downward marine areas in terms of
41 nighttime chemistry. During the CAM period, nocturnal ozone was higher, while NO_x was
42 much lower. The NO₃ production was still very fast, with a rate of 1.2 ppbv h⁻¹. With the
43 absence of N₂O₅ measurement in this period, the NO₃ reactivity towards VOCs and N₂O₅
44 uptake were calculated to assess NO₃ loss processes. We showed that the average k(NO₃)
45 from VOCs (56.5%, 2.6 ± 0.9 × 10⁻³ s⁻¹) was higher than N₂O₅ uptake (43.5%, 2.0 ± 1.5 ×
46 10⁻³ s⁻¹) during the CAM period, indicating a longer NO₃/N₂O₅ lifetime than that during
47 IAM period. This study improves the understanding of the nocturnal NO₃ budget and
48 environmental impacts with the interaction of anthropogenic and natural activities in
49 marine regions.

50

51 1. Introduction

52 Reactive nitrogen compounds, especially the nitrate radical (NO₃) and dinitrogen pentoxide
53 (N₂O₅) play an essential role in nocturnal atmospheric chemistry (Wayne et al., 1991;
54 Brown and Stutz, 2012). NO₃ is mainly generated via the oxidation of NO₂ by O₃ (R1), and
55 then NO₃ further reacts with NO₂ to produce N₂O₅ (R2) with a thermal equilibrium. The
56 temperature-dependent equilibrium constant, K_{eq}, regulates the equilibrium favoring NO₃
57 and NO₂ at higher temperatures (Osthoff et al., 2007; Chen et al., 2022). During daytime,
58 the NO₃ mixing ratio is generally low as its lifetime is very short (< 5 s) due to the fast
59 photolysis (R3) and rapid reaction with NO (R4) (a rate constant of 2.6 × 10⁻¹¹ cm³
60 molecule⁻¹ s⁻¹ at 298 K; Atkinson et al., 2004). While at night, NO₃ accumulates and can
61 reach tens to hundreds of parts per trillion volume (pptv), making it the major nocturnal
62 oxidizing agent (Wang et al., 2015).





67 During nighttime, NO_3 is the most important oxidant for alkenes (Mogensen et al., 2015;
68 Edwards et al., 2017), particularly in rural, remote, or forested environments, where it
69 predominantly reacts with unsaturated biogenic volatile organic compounds (VOCs),
70 especially isoprene and monoterpene (Ng et al., 2017; Liebmann et al., 2018b; Liebmann
71 et al., 2018a), to form alkyl nitrates (RONO_2), that ultimately lead to secondary organic
72 aerosols (SOAs) (Brown and Stutz, 2012). The observations and model simulations showed
73 that the measured particulate organic nitrates were largely attributed to the nocturnal NO_3
74 oxidation across Europe (Kiendler-Scharr et al., 2016). The NO_3 oxidation was also
75 reported to play an important role in aerosol formation in the Southeastern United States
76 with high isoprene and monoterpene emissions (Xu et al., 2015). These studies highlighted
77 the critical role of the reaction of NO_3 with VOCs in NO_3 budget and organic aerosol
78 pollution. In addition, NO_3 also reacts with dimethyl sulfide (DMS) over the ocean,
79 affecting the marine sulfur cycle and thus cloud formation and global climate (Aldener et
80 al., 2006; Brown and Stutz, 2012; Ian Barnes et al., 2006; Rosati et al., 2022). While in
81 high aerosol loading regimes, the N_2O_5 heterogeneous uptake becomes a significant
82 indirect NO_3 loss pathway. The hydrolysis reaction produces nitrate (NO_3^-) and nitryl
83 chloride (ClNO_2) on chloride-containing aerosols surfaces (Osthoff et al., 2008; Thornton
84 et al., 2010), in which ClNO_2 activates the Cl radical and further enhances the
85 photochemistry and ozone pollution in the following day (Riedel et al., 2012; Riedel et al.,
86 2014; Behnke et al., 1993).

87 Different NO_3 loss pathways produce different air pollutants and cause different
88 environmental impacts, characterization of NO_3 budget is essential to clarify the NO_3
89 chemistry in air pollution under various environments. Observations of N_2O_5 and NO_3 in
90 different regions and evaluation of their loss processes have been reported in numerous
91 studies (Crowley et al., 2011; Geyer et al., 2001; Brown et al., 2011; Dewald et al., 2022;
92 Niu et al., 2022; Brown et al., 2016; Wang et al., 2020a; Tham et al., 2016; Aldener et al.,
93 2006; Lin et al., 2022). In general, the NO_3 loss process shows significant regional
94 differences. In urban areas featuring intensive anthropogenic NO_x emissions and moderate
95 (or high) aerosol loading, N_2O_5 uptake is comparable or even dominates the NO_3 loss
96 (Wang et al., 2013). While in rural and forested areas with abundant biogenic VOCs
97 (BVOC) emissions, the NO_3 loss processes were usually dominated by BVOCs (Dewald
98 et al., 2022; Geyer et al., 2001; Brown et al., 2011). As for the coastal areas, which were
99 jointly affected by the polluted air mass from the inland and the relatively clean air mass
100 from the ocean, the dominant NO_3 loss process varies greatly depending on the air mass
101 origin (Aldener et al., 2006; Niu et al., 2022; Brown et al., 2016; Crowley et al., 2011). For
102 instance, Crowley et al. (2011) found in the Atlantic coast of Southern Spain (forested area)
103 that when the air mass mainly originated from the Atlantic, NO_3 was mainly consumed by
104 BVOCs (mainly monoterpenes) emitted from nearby forests, while when the air mass came



105 from the continent, NO_3 loss was mainly due to reactions with anthropogenic VOCs
106 (AVOCs).

107 China has been recently proven to be a hot spot of nocturnal chemistry with a high NO_3
108 production rate (Wang et al., 2023). Many studies have reported the mechanisms, budget,
109 or impacts of NO_3 - N_2O_5 chemistry in different regions, while most of them were conducted
110 in urban regions (Wang et al., 2013; Yan et al., 2021; Wang et al., 2020a; Wang et al., 2017c;
111 Wang et al., 2017d). For example, Wang et al. (2017b) showed a significant contribution
112 of N_2O_5 uptake to nitrate pollution in summer and winter, and they also highlighted the fast
113 organic nitrate production rate observed in Beijing rural region in summer (Wang et al.,
114 2018b). Only several studies focused on nighttime oxidation in coastal cities like Shanghai,
115 Shenzhen, and Hong Kong (Zhu et al., 2022; Niu et al., 2022; Yan et al., 2019), which
116 showed different patterns of NO_3 chemistry compared with urban regions. Even fewer field
117 studies were conducted on the island which is far away from the coastal cities where the
118 interactions of the oceanic atmosphere and urban plumes can significantly affect the NO_3
119 budget and impacts. Given the diversity of air masses in inland and coastal areas, studies
120 are needed to gain a comprehensive understanding of NO_3 losses in different atmospheric
121 environments, particularly in coastal and marine areas.

122 Therefore, we conducted an intensive field observation on Da Wan Shan Island (DWS) in
123 the winter of 2021, which is a typical island site in the north of the South China Sea, and
124 downward of the city clusters in the Pearl River Delta, China during the winter monsoon
125 periods. The island features a subtropical oceanic monsoon climate, and the north and
126 northeast synoptic winds from inland PRD and eastern China coast are generally
127 predominant in winter (Liu et al., 2019; Wang et al., 2018a). This allows us to further
128 investigate the interactions between anthropogenic emissions and marine emissions from
129 the perspective of nighttime chemistry. In this study, the measurements of N_2O_5 and the
130 related species observed during the DWS winter campaign are reported. We have identified
131 two types of air masses from both mainland China and coastal areas. Finally, the NO_3
132 budget and loss processes in different air masses are characterized.

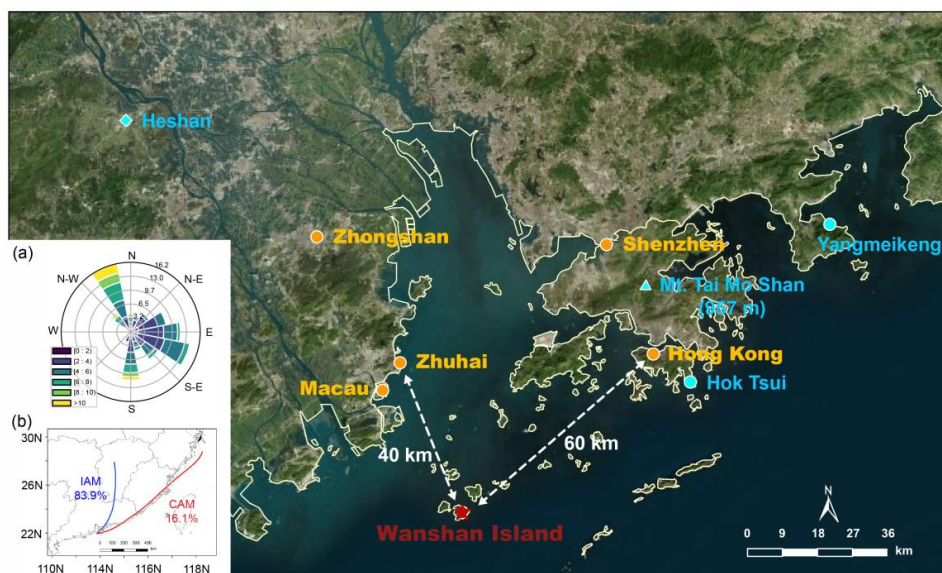
133 **2. Methods**

134 **2.1 Site description**

135 The field campaign was conducted at Da Wan Shan Island (21.93°N , 113.72°E) from Nov.
136 9th to Dec. 16th, 2021. Fig. 1 shows the study site, which is approximately 60 km southwest
137 of Hong Kong; 40 km southeast of Zhuhai; and about 100 km and 80 km away from the
138 megacities Guangzhou and Shenzhen, respectively. This island is dominated by



139 mountainous terrain with an area of 8.1 km² and has a small population of about 3000.
 140 Anthropogenic emissions are sparse and no industrial pollution sources were identified,
 141 though numerous ships engaging in local fishing activities were observed, potentially
 142 affecting the local atmosphere. During the measurement, local airflow was consistent from
 143 the northwest to southeast (Fig. 1a) due to the winter monsoon, with wind speeds most
 144 frequently ranging from 1.8 to 7.9 m s⁻¹ (10th - 90th percentiles) and an average of 4.5 ± 2.6
 145 m s⁻¹. This wind direction is indicative of the mixing of air masses from both continental
 146 and coastal areas. The HYbrid Single-Particle Lagrangian Integrated Trajectory model
 147 (HYSPLIT) was adopted to investigate the historical trajectory. The HYSPLIT model was
 148 run for 48 hours backward in time at local times of 20:00, 24:00, and 04:00, and at a height
 149 of 70 m above sea level. It confirmed that the air mass during nighttime mostly came from
 150 continental China (defined as inland air mass, IAM, 84%) and the coastal areas (defined as
 151 coastal air mass, CAM, 16%). No air masses free of pollution from the South China Sea
 152 were observed during the measurement period. All measurement instruments were placed
 153 in the DWS Atmospheric-Marine Research Station, located on the rooftop with inlets
 154 approximately 10 m above ground level and about 72 m above sea level. All times were
 155 given in CNST (Chinese National Standard Time = UTC + 8 h), with sunrise around 06:40
 156 CNST and sunset at 17:40 CNST.



157

158 **Figure 1.** A map of the field measurement site of Wanshan Island (red star) and the
 159 surrounding environment (extracted from BingSatelliteMap). Two coastal sites Hok Tsui
 160 (Yan et al., 2019) and Yangmeikeng (Niu et al., 2022), and an urban site Heshan (Wang et



161 al., 2022; Yun et al., 2018b) are denoted as blue circle and diamond, respectively. The blue
162 triangle denoted Mt. Tai Mo Shan (957 m), a mountainous site that studied the nighttime
163 chemistry in the nocturnal residual layer (Brown et al., 2016). The inset plot (a) provides
164 the wind rose for the sampling site during the campaign. Panel (b) shows the clustering
165 result of the 48-hrs backward trajectory calculations using the HYSPLIT model throughout
166 the campaign.

167 2.2 Instrument setup

168 Various parameters were measured in this study, including N_2O_5 , NO, NO_2 , O_3 , VOCs,
169 particle number size distribution (PNSD), and meteorological parameters with different
170 instruments. The detail information about these instruments is listed in Table 1. The N_2O_5
171 measurements were performed using a cavity-enhanced absorption spectrometer (CEAS)
172 which has been deployed in several field campaigns (Wang et al., 2017a; Wang et al., 2017b;
173 Wang et al., 2018b; Wang et al., 2020b). In brief, ambient N_2O_5 was thermally decomposed
174 to NO_3 in a perfluoro alkoxy alkane (PFA) tube (length: 35 cm, I.D.: 4.35 mm) heated to
175 $130\text{ }^\circ\text{C}$, and NO_3 was detected within a $110\text{ }^\circ\text{C}$ PFA resonator cavity. NO was injected to
176 destroy NO_3 from N_2O_5 thermal decomposition every 5 min cycle, and the result was used
177 as the reference spectrum to avoid the influence of ambient water vapor. A Teflon
178 polytetrafluoroethylene (PTFE) filter was used to remove ambient aerosol particles, and
179 the inlet flow rate was $1.0\text{ L}\cdot\text{min}^{-1}$. The loss of N_2O_5 in the sampling line and filter was
180 considered in the data correction. The limit of detection (LOD) was 2.7 pptv (1σ), and the
181 measurement uncertainty was $\pm 19\%$.

182 **Table 1.** The information of observation instruments used during the DWS campaign.

Species	Techniques	Detection limit	Accuracy	Time resolution
N_2O_5	CEAS	2.7 pptv (1σ)	$\pm 19\%$	10 s
NO	Chemiluminescence	0.4 ppbv	$\pm 5\%$	1 min
NO_2	Chemiluminescence	0.4 ppbv	$\pm 5\%$	1 min
O_3	UV photometry	0.4 ppbv	$\pm 5\%$	1 min
VOCs	PTR-TOF-MS	0.01 ppbv	$\pm 10\%$	10 s
PNSD	SMPS	5–300 nm	$\pm 10\%$	5 min

183 NO_x and O_3 were measured by commercial instruments (model T200U and model T400U,
184 Teledyne API Inc., respectively) calibrated with zero air before the measurement. The
185 nitrogen oxide analyzer uses the chemiluminescence detection method to measure the
186 original NO and converted NO_2 . Aerosol surface area density (S_a , $\mu\text{m}^2\text{ cm}^{-3}$) was calculated
187 based on the particle numbers and geometric diameter, which was measured by a



188 laboratory-assembled scanning-mobility particle sizer (SMPS). This SMPS system consists
189 of two differential mobility analyzers (DMA, "nano-DMA" mode 3081A, and "regular-
190 DMA" mode 3085A, TSI Inc.) in parallel, and a condensed particle counter (mode 3787,
191 TSI Inc.) as the detector. The combination of nano DMA and conventional mode 3085A
192 DMA enables the SMPS to have better detection performance for particles below 50 nm.
193 In this measurement, SMPS measured the particle size distribution in 5-300 nm with a time
194 resolution of 5 minutes, and S_a can be regarded as the lower limit value. A growth factor
195 $f(\text{RH}) = 1 + 8.8 \times (\text{RH}/100)^{9.7}$ (Liu et al., 2013) was used here to correct dry state S_a to wet
196 state S_a .

197 VOCs were measured by proton transfer reaction time of flight mass spectrometry (PTR-
198 TOF-MS, Ionicon Analytik GmbH, Innsbruck, Austria) with a time resolution of 10 s.
199 Meanwhile, VOCs were also sampled every 2 h using 2 L canisters on the selected days
200 when the hourly O_3 mixing ratio exceeded 70 ppbv, and the canister samples were analyzed
201 by a gas chromatograph equipped with a mass spectrometer or flame ionization detector
202 (GC-MS). For the absence of nocturnal data from canister samples, the following analysis
203 was based on the PTR-TOF-MS measurement. Since monoterpene species cannot be
204 distinguished by PRT-TOF-MS, the reaction rate constant of the sum monoterpene with
205 NO_3 was weighted by the campaign-averaged percentage of α -pinene and β -pinene
206 detected by GC-MS. Meteorological parameters (i.e., temperature (T), relative humidity
207 (RH), wind speed, and wind direction) were routinely monitored with a time resolution of
208 5 min.

209 2.3 The calculation of NO_3 budget and lifetime

210 With the observation of N_2O_5 , NO_3 can be calculated according to their temperature-
211 dependent equilibrium relationship (Eq. 1) (Brown and Stutz, 2012). The production rate
212 of nitrate radical, $\text{P}(\text{NO}_3)$, is commonly expressed by Eq. 2, where $k_{\text{NO}_2+\text{O}_3}$ represents the
213 temperature-dependent reaction rate constant of NO_2 and O_3 (Atkinson et al., 2004). In
214 general, the nocturnal NO_3 losses typically include three main pathways: (1) the reaction
215 with NO , (2) the reactions with VOCs, and (3) N_2O_5 uptake.

$$216 \quad [\text{NO}_3] = [\text{N}_2\text{O}_5]/\text{Keq}(T)[\text{NO}_2]$$

$$217 \quad \text{Keq} = 5.50 \times 10^{-27} \times \exp(10724/T) \quad (\text{Eq. 1})$$

$$218 \quad \text{P}(\text{NO}_3) = k_{\text{NO}_2+\text{O}_3}[\text{O}_3][\text{NO}_2] \quad (\text{Eq. 2})$$

$$219 \quad \text{L}(\text{NO}_3) = \sum k_i[\text{VOC}_i][\text{NO}_3] + k_{\text{NO}+\text{NO}_3}[\text{NO}][\text{NO}_3] + k_{\text{het}}[\text{N}_2\text{O}_5] \quad (\text{Eq. 3})$$



220 The NO_3 reactivity towards VOCs, $k(\text{NO}_3)$, is the first-order loss rate coefficient
221 calculated from the products of the bimolecular rate coefficients k_i and the VOC
222 concentrations as shown in Eq. 4.

$$223 \quad k(\text{NO}_3) = \sum k_i[\text{VOC}_i] \quad (\text{Eq. 4})$$

224 The k_{het} is the first-order loss rate coefficient of N_2O_5 uptake on the aerosol surface. It
225 depends on the uptake coefficient $\gamma(\text{N}_2\text{O}_5)$, the aerosol surface area density S_a ($\mu\text{m}^2 \text{cm}^{-3}$),
226 and the mean molecular speed c (Eq. 5). The $\gamma(\text{N}_2\text{O}_5)$ is influenced by chemical
227 composition, physical properties of aerosol, as well as ambient conditions including related
228 humidity and temperature (Yu et al., 2020; Wagner et al., 2013; Wang et al., 2018b; Bertram
229 and Thornton, 2009; Tang et al., 2014; Kane et al., 2001). Here $\gamma(\text{N}_2\text{O}_5)$ is parameterized
230 based on RH and temperature (Eq. 6) (Hallquist et al., 2003; Kane et al., 2001; Evans and
231 Jacob, 2005).

$$232 \quad k_{het} = \frac{1}{4} c S_a \gamma(\text{N}_2\text{O}_5) \quad (\text{Eq. 5})$$

$$233 \quad \gamma(\text{N}_2\text{O}_5) = \alpha \times 10^\beta$$

$$234 \quad \alpha = 2.79 \times 10^{-4} + 1.3 \times 10^{-4} \times \text{RH} - 3.43 \times 10^{-6} \times \text{RH}^2 + 7.52 \times 10^{-8} \times \text{RH}^3$$

$$235 \quad \beta = 4 \times 10^{-2} \times (T - 294) \quad (T > 282\text{K})$$

$$236 \quad \beta = -0.48 \quad (T < 282\text{K}) \quad (\text{Eq. 6})$$

237 Lifetimes are commonly expressed as the ratio of their concentrations to the NO_3
238 production rate as determined by Eq. (7) and Eq. (8), assuming the production and loss are
239 in dynamic balance at night (Brown et al., 2003; Brown and Stutz, 2012).

$$240 \quad \tau_{\text{N}_2\text{O}_5} = \frac{[\text{N}_2\text{O}_5]}{P(\text{NO}_3)} = \frac{[\text{N}_2\text{O}_5]}{k_{\text{NO}_2+\text{O}_3}[\text{NO}_2][\text{O}_3]} \quad (\text{Eq. 7})$$

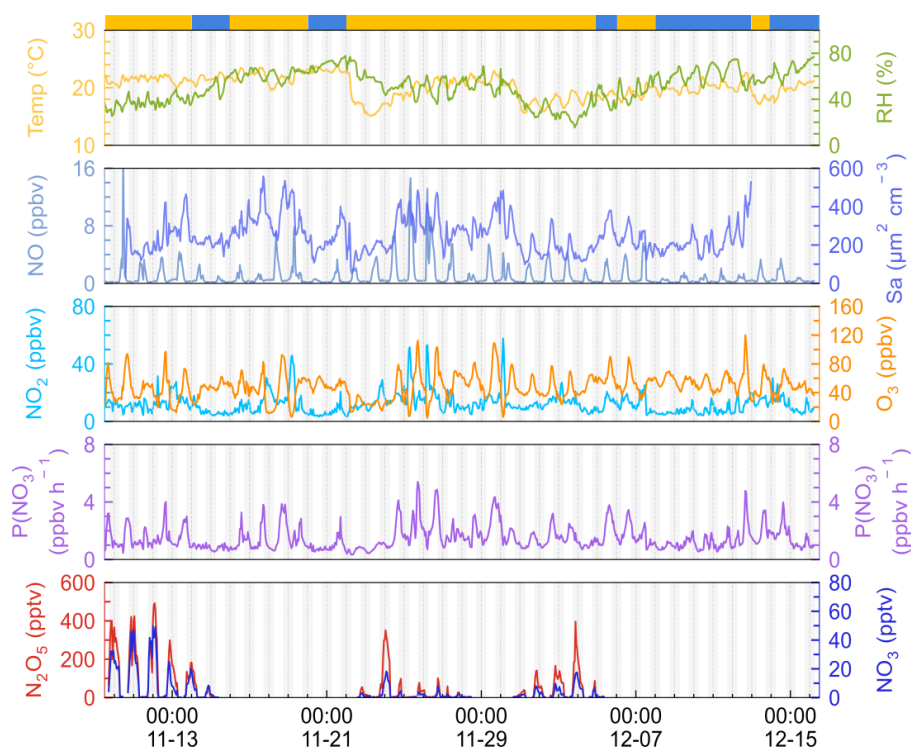
$$241 \quad \tau_{\text{NO}_3} = \frac{[\text{NO}_3]}{P(\text{NO}_3)} = \frac{[\text{NO}_3]}{k_{\text{NO}_2+\text{O}_3}[\text{NO}_2][\text{O}_3]} \quad (\text{Eq. 8})$$

242 **3. Results and discussion**

243 **3.1 Measurement overview**



244 The time series of N_2O_5 , related trace gases, and selected meteorological parameters for
 245 the study period are depicted in Fig. 2. The air masses are categorized into IAM and CAM
 246 according to the backward trajectories at 20:00, 00:00, and 04:00 each day as illustrated in
 247 Fig. 1. The detailed information of two kinds of air masses is listed in Table 2. Data gaps
 248 for N_2O_5 were caused by technical problems, mirror reflectivity calibration, or instrumental
 249 maintenance, which usually took place in the daytime. In this campaign, meteorological
 250 conditions featured a typical subtropical winter climate with average temperature and RH
 251 values of $20.1 \pm 1.9 \text{ }^\circ\text{C}$ and $52.0\% \pm 13.6\%$, respectively.



252

253 **Figure 2.** Time series of N_2O_5 , NO_3 , $\text{P}(\text{NO}_3)$, NO , NO_2 , Sa , temperature, and relative
 254 humidity in 1-hour average. The light gray shadow indicates the nighttime period. The
 255 ribbon at the top separates the air masses into two categories, yellow for inland air masses
 256 (IAM) and blue for coastal air masses (CAM).

257 Ozone exhibited the characteristic of afternoon photochemical peaks especially when the
 258 air mass comes from the inland. The average and maximum concentrations of ozone were
 259 $48.2 \pm 18.2 \text{ ppbv}$ and 120.1 ppbv , respectively, among which the hourly maximum level
 260 exceeded the Chinese national air quality standard ($200 \text{ } \mu\text{g m}^{-3}$, equivalent to 93 ppbv) for
 261 6 days out of 37 days of measurements. All these O_3 pollution episode days occurred during
 262 the IAM period. Meanwhile, the mixing ratio of NO , NO_2 , and Sa usually increased during



263 these days, indicating that this site was strongly affected by regional transport from inland
 264 China, i.e., the PRD region. Previous observations by Wang et al. (2018a) also found high
 265 O₃ levels in autumn on the same island due to the weak NO titration and high O₃ production
 266 rate. Detailed analysis of ozone and VOCs will be subjected to another manuscript (Fang
 267 et al., 2023).

268 Nitrogen oxides (NO_x = NO + NO₂) were at a moderate level with an average value of 13.1
 269 ± 8.2 ppbv, which is much lower than the values in PRD regions (usually > 20 ppbv, Wang
 270 et al., 2022; Yang et al., 2022; Yun et al., 2018b) and higher than those on the remote islands
 271 in South China Sea (< 5 ppbv, Chuang et al., 2013). The mixing ratio of NO at nighttime
 272 was low and showed small peaks during daytime. With the O₃ accumulating throughout
 273 the day, NO decreased to below the instrument detection limit in the first half of the night,
 274 while it began to increase as the O₃ concentration decreased in the second half of the night.
 275 Given that the lifetime of NO is only a few minutes in the presence of several tens of ppbv
 276 of O₃ (Dewald et al., 2022), NO is likely to come from a local source such as soil emission.

277 **Table 2.** Summary of detailed information on the two air mass types (mean ± standard
 278 deviation).

Species	IAM		CAM	
	All day	Nighttime	All day	Nighttime
O ₃ (ppbv)	45.8 ± 20.2	42.9 ± 18.4	53.1 ± 11.9	51.4 ± 9.6
NO _x (ppbv)	15.1 ± 8.7	14.5 ± 9	9.2 ± 5.1	8.8 ± 4.8
NO ₂ (ppbv)	13.9 ± 7.6	14.1 ± 8.3	8.6 ± 4.8	8.6 ± 4.8
NO (ppbv)	1.2 ± 2.3	0.4 ± 1.1	0.5 ± 0.6	0.2 ± 0.1
Temp (°C)	19.9 ± 2	19.9 ± 1.9	20.8 ± 1.5	20.6 ± 1.5
RH (%)	46.7 ± 12.5	47.7 ± 13.2	61.2 ± 10	64.1 ± 9.6
P(NO ₃) (ppbv h ⁻¹)	1.6 ± 0.9	1.5 ± 0.8	1.3 ± 0.8	1.2 ± 0.6
N ₂ O ₅ (pptv)	-	119.5 ± 128.6	-	-
NO ₃ (pptv) ^a	-	9.9 ± 12.5	-	-
τ _{N₂O₅} (min)	-	6.5 ± 6.5	-	-
τ _{NO₃} (min)	-	0.5 ± 0.7	-	-

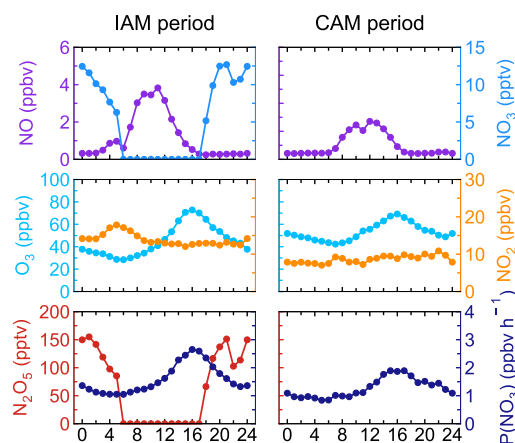
279 Note: ^a NO₃ is calculated by the thermal equilibrium between NO₂, NO₃, and N₂O₅.

280 N₂O₅ was at a moderate level on most days with a nocturnal average of 119.5 ± 128.6 pptv,
 281 with high concentrations (>400 pptv in 1-hour average) only lasting for three days. During
 282 the nights from November 9th to 12th, the N₂O₅ concentrations were significantly higher
 283 than those at other nights, with a maximum of 657.3 pptv at midnight of November 12th.
 284 The NO₃ concentration (calculated based on the thermal equilibrium with N₂O₅) was also
 285 moderate with an average mixing ratio of 9.9 ± 12.5 pptv, which was higher than that



286 reported on a nearby coastal site of Hong Kong Island (Yan et al., 2019). Table 3 compares
287 the N_2O_5 , NO_3 , and $\text{P}(\text{NO}_3)$ found in other coastal (or island) and continental regions from
288 Europe, the United States, and China. In our study, N_2O_5 and NO_3 were at a moderate level
289 compared to other coastal regions when they were affected by emission plumes from
290 continental regions, such as Northwestern Europe (Morgan et al., 2015), the East coast of
291 the USA (Brown et al., 2004), and Shenzhen, China (Niu et al., 2022), and were comparable
292 with urban regions (Wang et al., 2017b; Wang et al., 2018b). The concentrations of NO_3
293 precursors (NO_2 and O_3) at this site were much similar to some rural areas, leading to a
294 high NO_3 production rate with a daily average of 1.5 ± 0.9 ppbv h^{-1} and a maximum of 5.9
295 ppbv h^{-1} . The average value is much higher than that reported in Beijing in winter (0.4 ppbv
296 h^{-1} , (Wang et al., 2021), comparable to autumn (1.4 ± 1.7 ppbv h^{-1} , (Wang et al., 2017b) and
297 even higher than that in summer Taizhou (1.01 ± 0.47 ppbv h^{-1} , (Wang et al., 2020a). The
298 nocturnal $\text{P}(\text{NO}_3)$ was 1.4 ± 0.7 ppbv h^{-1} , even higher than the average value in the warm
299 season of China with 1.07 ± 0.38 ppbv h^{-1} (Wang et al., 2023). Besides the high NO_2 and
300 O_3 , the high reaction rate constant for NO_2 and O_3 due to the high temperature at this site
301 is a potential explanation for the high $\text{P}(\text{NO}_3)$ values observed in this study. The high $\text{P}(\text{NO}_3)$
302 and the low concentrations of N_2O_5 and NO_3 indicate intensive atmospheric oxidation
303 capacity and fast NO_3 and N_2O_5 removal over the Pearl River Estuary.

304 The difference of trace gases in IAM and CAM periods, and the mean diurnal profiles of
305 N_2O_5 , together with relevant species are shown in Fig. 3. Daytime N_2O_5 and NO_3 in the
306 IAM period were shown as zero due to the absence of observation. Because of limited N_2O_5
307 data for the CAM period, neither N_2O_5 nor NO_3 is shown in Fig. 3. NO exhibited similar
308 diurnal variation in both periods and the mixing ratio was higher in the IAM period. The
309 wind rose plot (Fig. S1) showed high concentrations of NO originating from the north
310 characterized by the outflow from PRD regions. However, NO_2 differed in the two periods,
311 showing highly anti-correlation with O_3 only in the IAM period and little diurnal variation
312 in the CAM period. A fit of nocturnal O_3 against NO_2 (Fig. S2) yields a slope of -1.1 in
313 IAM, implying that the major emission of NO_x was NO and almost no nocturnal NO_2
314 production occurred (Brown et al., 2016).



315
 316 **Figure 3.** Mean diurnal profiles of N_2O_5 , $P(NO_3)$, and relevant parameters in the two types
 317 of air masses.

318 Ozone exhibited a typical diurnal pattern for all airmasses, gradually increasing until its
 319 peak at 16:00 and then slowly decreasing throughout the night until its lowest mixing ratio
 320 was reached at about 06:00. Compared to the CAM period, the lower minimum hourly O_3
 321 concentration and a small peak of NO_2 in the early morning indicated that NO titration
 322 effect was stronger in the IAM period, and the higher maximum of O_3 concentration in
 323 IAM indicated that photochemical formation of O_3 and/or transport was faster to
 324 completely offset the titration. In addition, the higher NO_x and VOC concentrations in the
 325 IAM period facilitated O_3 formation. With the elevated precursor concentrations (NO_2 and
 326 O_3) in the IAM period, N_2O_5 and NO_3 accumulated rapidly after sunset, reaching their peak
 327 values (155.0 pptv for each) near 20:00. $P(NO_3)$ was highly consistent with O_3 in diurnal
 328 variation and reached the peak at 16:00, with peak values of 2.7 ppbv h^{-1} (IAM) and 1.9
 329 ppbv h^{-1} (CAM), as well as a nocturnal average value of $1.5 \pm 0.8 \text{ ppbv h}^{-1}$ (IAM) and 1.2
 330 $\pm 0.6 \text{ ppbv h}^{-1}$ (CAM), respectively. The $P(NO_3)$ of CAM was consistent with the
 331 observation in eastern Shenzhen ($1.2 \pm 0.3 \text{ ppbv h}^{-1}$) (Niu et al., 2022) during which the air
 332 masses were transported from clean areas or the sea surface.



Table 3. Summary of field-observed N₂O₅, NO₂, O₃ concentrations, and NO₃ production rate.

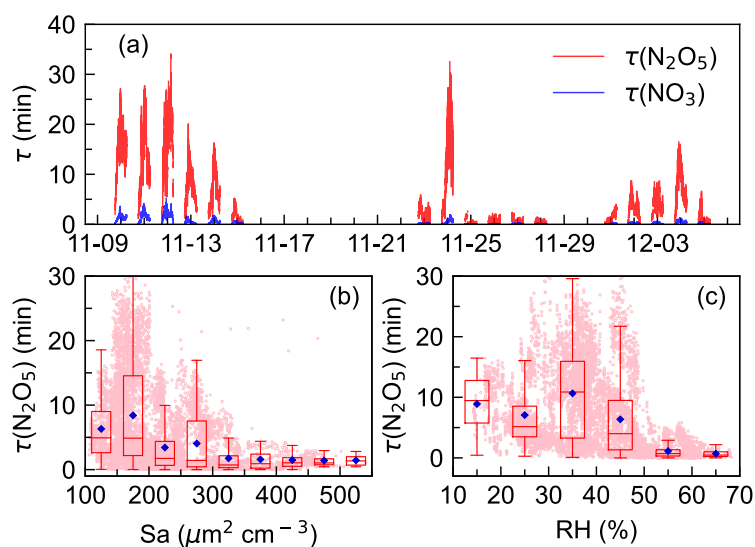
Region	Location	Time	N ₂ O ₅ (pptv)	NO ₂ (pptv)	NO ₃ (ppbv)	O ₃ (ppbv)	P (NO ₃) (ppbv hr ⁻¹)	References
Urban	Jinan, China	Aug.-Sep., 2014	22 ± 13 (max 278)	74.6	55	/	(Wang et al., 2017c)	
Urban	Shanghai, China	Aug.-Oct., 2011	310 ± 380	0-76	23 ± 8 (max 57)	1.10 ± 1.09	(Wang et al., 2013)	
Urban	Beijing, China	May-Jul., 2016	100-500 (max 937)	/	/	1.2 ± 0.9	(Wang et al., 2018b)	
Urban	Mt. Tai, China	Jul.-Aug., 2014	6.8 ± 7.7	16.4 (±6.1)	88.6 (±16.6)	0.45 ± 0.40	(Wang et al., 2017d)	
Urban	Heshan, China	Sep.-Nov., 2019	64 ± 145 (night) (max 1180)	max 90	75.2 ± 20.9 (max 152.8)	2.5 ± 2.1 (day) 1.8 ± 1.5 (night)	(Wang et al., 2022)	
Urban	Beijing, China	Sep.-Oct., 2019	68.0 ± 136.7	/	35.1 ± 16.6	27.7 ± 25.2	2.25 ± 2.02	(Wang et al., 2017b)
Suburban	Changzhou, China	May-Jul., 2019	53.4 ± 66.1 (max 304.7)	4.7 ± 3.5 (max 17.7)	48.4 ± 27.8	1.7 ± 1.2 (max 7.7)	(Lin et al., 2022)	
Rural	Wangdu, China	Jun.-Jul., 2014	<200 (max 430)	/	10-80	1.7 ± 0.6	(Tham et al., 2016)	
Rural	Taizhou, China	May-Jul., 2018	26.0 ± 35.7 (max 492)	4.4 ± 2.2 (max 150)	48.2 ± 32.5	1.01 ± 0.47 (night)	(Wang et al., 2020a)	
Coastal	Tai Mo Shan, HK	Nov.-Dec., 2013	0.5-11.8 ppbv	-	7.88	68.5	0.01-2	(Brown et al., 2016)
Coastal	East coast of USA	Jun.-Aug., 2002	85	17	6	35	/	(Brown et al., 2004)
Coastal	California, USA	Jan., 2004	0-200	/	0-15	15-35	/	(Wood et al., 2005)
Coastal	Southern Spanish	Nov.-Dec., 2018	~500 (max)	/	1-15	15-40	/	(Crowley et al., 2011)
Coastal	Shenzhen, China	Sep.-Oct., 2019	55.6 ± 89 (max 1420)	/	6.2	88.9 ± 24.6	2.9 ± 0.5 (UAM)	(Niu et al., 2022)
Coastal	Northwestern Europe	Jul., 2010	45.4 ± 55.2 (BAM)	/	0.5-2	30-40	1.2 ± 0.3 (BAM)	(Morgan et al., 2015)
Island	Hok Tsui, HK	Aug.-Sep., 2012	17 ± 33 (max 336)	7 ± 12	6 ± 7	33 ± 24	/	(Yan et al., 2019)
Island	Wanshan, China	Nov.-Dec., 2021	107.22 ± 125.17	7.56 ± 10.95	13.14 ± 8.68	43.75 ± 18.49	1.38 ± 0.83	This work

334 Notes: UAM means air masses coming from continental areas, and BAM means air masses coming from background marine areas.
 335 Mean values are in the form of mean ± standard deviation or single data. The maximum was noted in the table.



336 3.2 The lifetimes of N_2O_5 and NO_3

337 Steady-state lifetime is one of the most common and useful diagnostics for NO_3 and N_2O_5
 338 analysis in the atmosphere (Brown et al., 2003; Wang et al., 2018b; Wang et al., 2020a;
 339 Brown et al., 2016). As shown in Fig. 4, τ_{NO_3} was low during the whole campaign with
 340 an average of 0.5 ± 0.7 min. $\tau_{N_2O_5}$ showed a similar pattern to τ_{NO_3} but had a much
 341 higher value, ranging from 0 to 34.1 min with an average of 6.1 ± 6.5 min. The N_2O_5
 342 lifetime was higher in the first half of the campaign (11.5 min, November 9th to 14th) than
 343 in the second half (3.5 min, November 22th to 28th). The difference was mainly due to the
 344 N_2O_5 mixing ratio rather than $P(NO_3)$, as $P(NO_3)$ shows no significant difference during
 345 the whole observation (Fig. 2).



346

347 **Figure 4.** Time series of N_2O_5 and NO_3 lifetimes (a) and variations of nocturnal N_2O_5
 348 lifetime as a function of aerosol surface area density, S_a (b), and relative humidity, RH (c).
 349 The blue diamond represents the average $\tau_{N_2O_5}$ and pink dots represent the scatter data
 350 point in 1 min.

351 $\tau_{N_2O_5}$ values were comparable to those measured on the coastline of Finokalia, Greece for
 352 a median of 5 min (Vrekoussis et al., 2004; Vrekoussis et al., 2007), but much lower than
 353 those previously reported in the residual layer in Hong Kong for 1-5 h (Brown et al., 2016).
 354 In comparison, the lifetimes were much longer than in inland urban areas, for example,
 355 0.93 ± 1.13 min in Taizhou (Li et al., 2020), 1.6 ± 1.5 min in Changzhou (Lin et al., 2022)
 356 for YRD regions, 1.1-10.7 min (Zhou et al., 2018) and 4.5 ± 4.0 min (Wang et al., 2018b)



357 in Beijing. Typically, high aerosol loading, more intensive VOC, and NO emissions in these
358 areas led to enhanced N₂O₅ uptake and reactions of NO₃ with VOC. But at this site, the
359 atmosphere was relatively clean since the maximum S_a value was less than 600 μm² cm⁻³,
360 making N₂O₅ uptake slow. Fig. 4b shows N₂O₅ lifetime decreased rapidly from 8.3 min to
361 1.7 min when S_a increased up to 300 μm² cm⁻³ and then remained at relatively low constant
362 levels though S_a still increased. Such a trend of τ_{N₂O₅}-S_a dependence was consistent with
363 previous observations and varied in exact values (Zhou et al., 2018; Wang et al., 2018b; Li
364 et al., 2020). Fig. 4c. showed that τ_{N₂O₅} decreased as RH increased (> 40%) possibly due
365 to the hygroscopic aerosol growth and the dependence of the N₂O₅ uptake coefficient on
366 the RH (Brown and Stutz, 2012). Overall, the trend is consistent with previous works, while
367 the large discrepancy of the dependence implied that N₂O₅ uptake was not the dominant
368 NO₃ loss process.

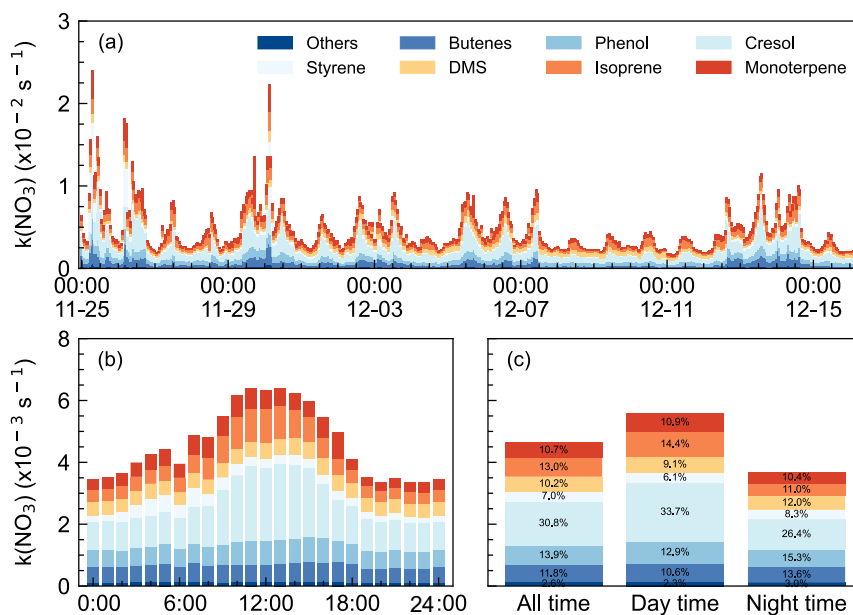
369 3.3 The NO₃ reactivity and N₂O₅ uptake coefficients

370 The concurrent high P(NO₃) and low NO₃ lifetime imply high NO₃ reactivity as well as a
371 large nocturnal NO₃ loss process at DWS. The NO₃ reactivity (k(NO₃)) towards VOCs was
372 calculated by Eq. 4, towards which were categorized into anthropogenic VOC and biogenic
373 VOC. Throughout the campaign, k(NO₃) varied considerably (Fig. 5a), showing relatively
374 high and fluctuated values when the airmasses featured IAM. The k(NO₃) ranged from 1.6
375 × 10⁻³ s⁻¹ to 2.4 × 10⁻² s⁻¹ with the daily average of 4.6 ± 2.8 × 10⁻³ s⁻¹. Low values of k(NO₃)
376 were observed from December 9th to 12th when the air masses originate from coastal or
377 offshore from the east and southeast, which features the outflow of coastal cities like Hong
378 Kong and Shenzhen.

379 Fig. 5b shows the mean diurnal profile of k(NO₃), where a trend of high values in the
380 daytime and low values at nighttime are observed. Anthropogenic VOC, especially cresol,
381 dominated the daily trend of k(NO₃), while biogenic VOC-k(NO₃) showed no significant
382 diurnal variation. Except cresol, other highly reactive VOC showed little change
383 throughout the day. Regarding the biogenic VOC-k(NO₃), the concentrations of
384 monoterpene, isoprene, and DMS changed smoothly although their emissions would
385 increase with elevated temperature and sunlight during daytime (Fuentes. et al., 2000). The
386 detailed contributions of VOC categories to k(NO₃) were shown in Fig. 5c. The k(NO₃)
387 was 5.6 ± 2.8 × 10⁻³ s⁻¹ and 3.7 ± 2.5 × 10⁻³ s⁻¹ on average for daytime and nighttime,
388 respectively. The daytime distribution of k(NO₃) differed from that at the mountaintop of
389 Tai Mo Shan in Hong Kong (Brown et al., 2016). During the nighttime, anthropogenic
390 VOC-k(NO₃) tripled the biogenic VOC-k(NO₃) and was dominated by cresol (26.4%). The
391 nighttime k(NO₃) corresponded to a NO₃ lifetime of 4.5 min, which was about 10 times the
392 lifetime derived from steady-state analysis, indicating that the reaction of NO₃ with VOC



393 was not significant enough. The faster NO_3 loss rate also indicated the less aged air mass
 394 that was influenced by surface-level emissions.



395

396 **Figure 5.** NO_3 reactivity via VOCs during the campaign. (a) $k(\text{NO}_3)$ time series from Nov.
 397 25th to Dec. 15th; (b) mean diurnal profiles; and (c) the relative contribution in different
 398 categories.

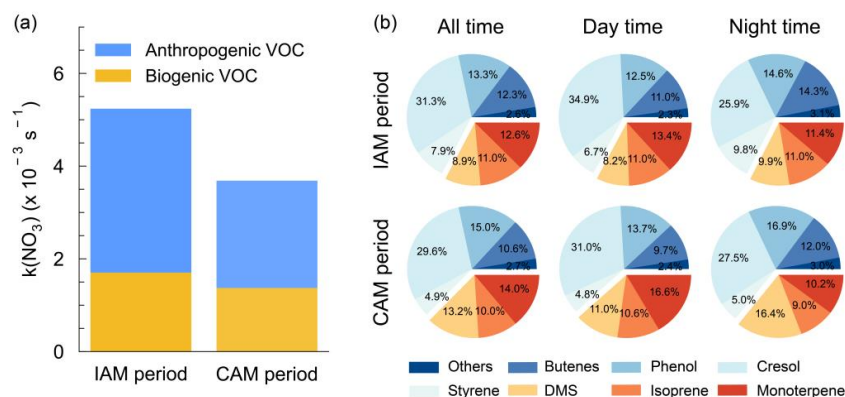
399 We showed that NO_3 reactivity and its composition in this study exhibited significant
 400 differences compared to other urban or forested regions (Wang et al., 2017d; Ayres et al.,
 401 2015; Brown et al., 2016; Lin et al., 2022). Although anthropogenic VOCs played a
 402 dominant role, accounting for 66.1%, the major contributors were not low-carbon alkenes
 403 but phenol and cresol, which have received little attention in previous studies. Despite their
 404 relatively low concentrations, averaging 7 ± 3 pptv and 4 ± 3 pptv respectively, their
 405 substantial contribution to $k(\text{NO}_3)$ is notable due to their fast rate constants ($3.8 \times 10^{-12} \text{ cm}^3$
 406 $\text{molecule}^{-1} \text{ s}^{-2}$ and $1.4 \times 10^{-11} \text{ cm}^3 \text{ molecule}^{-1} \text{ s}^{-2}$ at 298 K, respectively) for reaction with
 407 NO_3 . These substances are mainly secondary species from aromatic compounds and
 408 significantly higher concentrations have also been observed in urban areas (Delhomme et
 409 al., 2010; Zhu et al., 2005; Belloli et al., 1999). Hence, these phenolic compounds were
 410 potentially important but often overlooked for their contributions to NO_3 reactivity in urban
 411 areas, and their reactions with NO_3 may also contribute to the formation of nitrophenol.
 412 These reactions warrant further attention in future research. Regarding biogenic VOCs,



413 besides the contributors commonly observed in forest regions such as monoterpenes and
414 isoprene, the marine emissions indicator, dimethyl sulfide (DMS), contributed 10.2% to
415 NO₃ reactivity (daily average). Previous studies have suggested that DMS may serve as a
416 major direct sink for NO₃ in clean marine regions (Allan et al., 1999; Aldener et al., 2006;
417 Brown et al., 2007). However, this study reveals that anthropogenic VOC emissions
418 significantly enhanced the NO₃ reactivity in marine areas, highlighting the crucial influence
419 of anthropogenic activities on marine atmospheric chemistry.

420 As shown in Fig. 6a, $k(\text{NO}_3)$ differed significantly between the inland and coastal air
421 masses, with $5.2 \times 10^{-3} \text{ s}^{-1}$ and $3.7 \times 10^{-3} \text{ s}^{-1}$ on average in IAM and CAM periods,
422 respectively. Of which anthropogenic VOC- $k(\text{NO}_3)$ in IAM ($3.5 \times 10^{-3} \text{ s}^{-1}$) was higher than
423 in CAM ($2.3 \times 10^{-3} \text{ s}^{-1}$) and dominant in both air masses, while biogenic VOC- $k(\text{NO}_3)$ was
424 comparable. The difference indicated that this region was affected by long-range transport
425 emissions to a certain extent. The pie charts in Fig. 6b showed different VOC categories
426 that contributed to $k(\text{NO}_3)$ in two periods with AVOC dominant at any time. The change in
427 the relative contribution of various VOCs to $k(\text{NO}_3)$ varied simultaneously throughout the
428 day, reflecting as butene, phenol, and DMS increased, while cresol and monoterpene
429 decreased from daytime to nighttime.

430 N₂O₅ heterogeneous uptake on aerosol is one of the vital loss processes of NO₃ and the
431 uptake coefficient varied greatly under different environmental conditions. For instance,
432 $\gamma(\text{N}_2\text{O}_5)$ can reach up to 0.072 in polluted urban regions (Wang et al., 2017b; Wang et al.,
433 2018b; Lu et al., 2022; Li et al., 2020), while usually below 0.03 in coastal areas (Brown
434 et al., 2016; Morgan et al., 2015; Niu et al., 2022). N₂O₅ uptake coefficient can be gotten
435 from the pseudo steady state method by assuming that N₂O₅ and NO₃ have achieved a
436 steady state (Brown et al., 2009), in which the fitted slope represents $\gamma(\text{N}_2\text{O}_5)$ and the
437 intercept represents the direct loss rate coefficient, $k(\text{NO}_3)$. However, this approach failed
438 to generate valid results in our study since a negative slope or intercept was observed (Fig.
439 S3). These results indicated that a large NO₃ removal process existed at this site, making it
440 unable to approach a stable state. Based on relative humidity and temperature, we
441 calculated the uptake coefficient by Eq.6 from November 9th to 16th. The parameterized
442 average $\gamma(\text{N}_2\text{O}_5)$ showed a large variation ranging from 0.0014 to 0.0299, with an average
443 of 0.0095 ± 0.0059 . This value is within the range from <0.0016 to 0.03 derived from the
444 ambient observation around other coastal areas (Niu et al., 2022; Yun et al., 2018a; Brown
445 et al., 2006; Brown et al., 2016; Morgan et al., 2015) and smaller than the polluted North
446 China Plain (Wang et al., 2017c; Wang et al., 2017b; Wang et al., 2017d; Tham et al., 2018).



447

448 **Figure 6.** (a) Distributions of $k(\text{NO}_3)$ in continental and coastal air masses. (b) The relative
 449 contribution of VOC categories to the $k(\text{NO}_3)$.

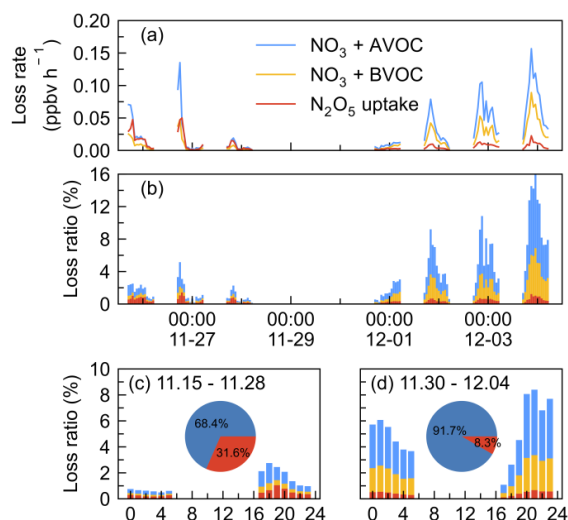
450 3.4 The NO_3 loss budget

451 To assess the contribution of various loss processes to the total NO_3 removal, we calculated
 452 their loss rate and the loss ratio, $LR(\text{NO}_3)$. Considering the short lifetime of NO_3 , here the
 453 total NO_3 loss is represented by $P(\text{NO}_3)$ which characterizes the atmospheric oxidation
 454 capacity of NO_3 to its reactants. Due to the data absence of measured VOCs or N_2O_5 during
 455 certain periods, the loss proportion of VOCs and N_2O_5 uptake in NO_3 loss only presented
 456 from Nov. 26th to Dec. 5th during which all air masses originated from continental China.
 457 As shown in Fig. 7, a closer examination revealed that the nights can be divided into two
 458 periods, period I: November 25th to 28th when the loss ratio of VOC and N_2O_5 uptake
 459 remained below 3%, and period II: November 30 to December 4 when the loss ratio was
 460 higher. Both periods had large nocturnal NO_3 production rates with an average of 2.1 ± 1.1
 461 ppbv h^{-1} in period I and $1.4 \pm 0.6 \text{ ppbv h}^{-1}$ in period II, respectively.

462 N_2O_5 uptake rate was larger in period I ($0.01 \pm 0.01 \text{ ppbv h}^{-1}$) than that in period II (0.006
 463 $\pm 0.004 \text{ ppbv h}^{-1}$), which can be explained by the increased RH, Sa, and N_2O_5 concentration
 464 as shown in Fig. 2. The loss ratio of these processes was shown in Fig. 7b, the total NO_3
 465 loss through reactions with VOCs and N_2O_5 uptake accounted for less than 20%, with an
 466 average of 1.2% (period I) and 5.3% (period II), respectively. This result shows that the
 467 nighttime NO_3 chemistry may be almost negligible, compared with the NO_x removal
 468 capacity during the day according to previous works reported in urban regions (Wang et
 469 al., 2017b; Wang et al., 2020a). The diurnal variation of the NO_3 loss fraction of both
 470 periods was shown in Fig. 7c and 7d, revealing that NO_3 loss via N_2O_5 uptake and VOCs



471 was slightly higher in the early evening and relatively stable in the late evening. The pie
 472 charts in the center were the relative contribution between VOCs and N₂O₅ uptake, showing
 473 that VOCs were overwhelming compared with N₂O₅ uptake during the two periods, with
 474 an average of 68.4% and 91.7% during the first and second periods, respectively.



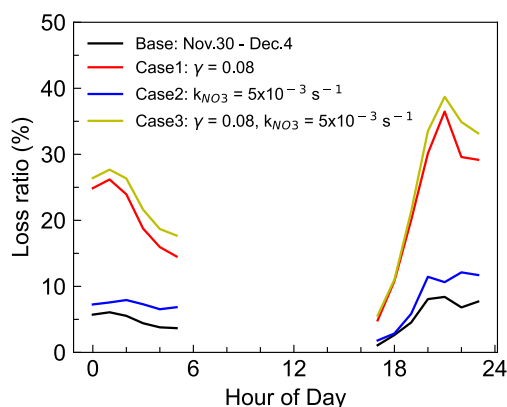
475

476 **Figure 7.** Time series of (a) the loss rate of NO₃ reactions with AVOC, BVOC, and N₂O₅
 477 uptake, and (b) fractional contribution to the NO₃ loss during the nighttime by taking
 478 P(NO₃) as the total NO₃ loss in the IAM period. The mean diurnal profiles of NO₃ loss
 479 ratio in two periods (c) November 25th - 28th, and (d) November 30th - December 4th. Pie
 480 charts in the center showed the relative contribution of VOCs (blue) and N₂O₅ uptake (red)
 481 in NO₃ loss.

482 Due to the difficulty in experimental quantifying $\gamma(\text{N}_2\text{O}_5)$, the estimation of N₂O₅ uptake
 483 in NO₃ loss may include some uncertainty. Considering the uncertainty both in
 484 parameterized $\gamma(\text{N}_2\text{O}_5)$ and the NO₃ reactivity calculation, three sensitivity tests were
 485 conducted to assess the uncertainty in period II because of the relatively high loss ratio in
 486 the above analysis (Fig. 8), and the three cases were used to represent the upper limit of
 487 their contribution to NO₃ loss. Case 1 represents the overrated contribution of N₂O₅ uptake
 488 by taking $\gamma(\text{N}_2\text{O}_5) = 0.08$, which was the high value reported in high N₂O₅ and ClNO₂
 489 plume of Shenzhen (Niu et al., 2022) and approximately seven times the parameterized
 490 value at this site. In this case, the fraction of NO₃+VOCs and N₂O₅ uptake was significantly
 491 elevated to account for approximately 30% of NO₃ loss. Case 2 shows the total NO₃
 492 reactivity reached an average of $5.0 \times 10^{-3} \text{ s}^{-1}$ by taking β -pinene as the total monoterpene
 493 because of the higher reaction rate constant. The weak change in the loss ratio indicates the



494 reactions of NO_3 with VOC may not be sensitive to the weights of monoterpenes, since the
 495 contribution of monoterpenes to the NO_3 reactivity is not dominant. Case 3 is the synthesis
 496 of Case 1 and Case 2 by considering higher N_2O_5 uptake coefficient and higher $k(\text{NO}_3)$ to
 497 represent the upper limit of N_2O_5 uptake and NO_3 reaction with VOCs to NO_3 loss, whose
 498 result is slightly higher than the contribution of Case 1. Nevertheless, the quantified upper
 499 contribution was still less than half. Thus, we conclude that most of the NO_3 loss was not
 500 well accounted for even considering the uncertainties.



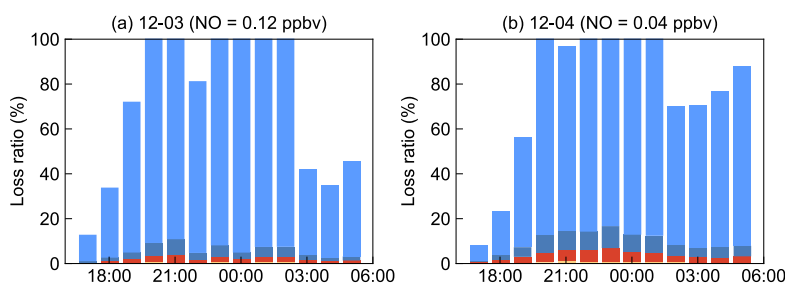
501

502 **Figure 8.** Three sensitivity tests for the contribution of VOCs and N_2O_5 uptake to the NO_3
 503 loss during the nighttime of period II (November 30th - December 4th). Case 1 takes $\gamma(\text{N}_2\text{O}_5)$
 504 = 0.08, which is the high value reported in the previous study. Case 2 takes β -pinene as the
 505 total monoterpene with a higher reaction rate constant, and Case 3 is the synthesis of the
 506 above two cases to represent the upper limit of the contribution.

507 The NO_3 reaction with NO was often considered to be one of the dominant loss processes
 508 during the daytime since at nighttime NO decreased to low levels, thus not considered in
 509 the above analysis. However, by taking NO into consideration although at low
 510 concentration levels below the detection limit of the instrument (0.4 ppbv), the contribution
 511 of NO to the nighttime NO_3 loss exceeded 100% frequently as shown in Fig. S4. Due to
 512 the rapid reaction between NO and NO_3 , several pptv concentrations of NO could
 513 effectively account for most NO_3 loss in a relatively clean coastal environment (Crowley
 514 et al., 2011). Nevertheless, limited by NO precise measurement, we considered the
 515 following assessments to understand the total NO_3 loss processes (Fig. 9). By assuming
 516 NO at a constant value of 40-400 pptv, more than 80% of the total NO_3 loss can be well
 517 explained. Although some loss remained unidentified, these results underline that NO,
 518 often considered to be important during daytime, was the predominant NO_3 loss way during
 519 nighttime at this study site. This also suggests accurate measurement of low NO



520 concentrations is crucial for identifying removal pathways of nocturnal NO₃ oxidants and
 521 has significant implications for nighttime atmospheric chemistry. We can infer that the
 522 nocturnal chemical NO₃ reactions would be largely enhanced once without NO emission
 523 in the open ocean after the air mass passes through this site, indicating the strong influences
 524 of the urban outflow to the downward marine areas with respect to nighttime chemistry.



525

526 **Figure 9.** Assessments for NO₃ loss process by assuming NO as constant values. Blue
 527 represents the contribution of NO and others are N₂O₅ uptake and VOCs.

528 For the absence of measured N₂O₅ during the CAM period, we compared the $k(\text{NO}_3)$ and
 529 the reactivity of N₂O₅ uptake ($k_{\text{het}}K_{\text{eq}}\text{NO}_2$) to indirectly reflect NO₃ removal process.
 530 Overall, the NO₃ reactivity values from VOCs and N₂O₅ uptake during nighttime was
 531 relatively comparable, for 56.5% and 43.5%, respectively. This indicates that VOCs still
 532 had a slightly larger contribution than N₂O₅ uptake during the CAM period, which is
 533 consistent with the findings in southern China (Brown et al., 2016) and on the east coast of
 534 the USA (Aldener et al., 2006).

535 4. Summary and Conclusion

536 This study presents the first observation of nocturnal nitrogen oxide species, N₂O₅, at a
 537 typical marine site (Da Wan Shan Island, Zhuhai) in the north of the South China Sea during
 538 the winter of 2021. Although Da Wan Shan Island was almost free of local anthropogenic
 539 emissions, the air pollutants from the megacities of the Pearl River Delta were transported
 540 to this area by northerly or northeasterly winds during the measurement period. The
 541 maximum ratio of N₂O₅ was 657.27 pptv (1 min average) and the nocturnal average was
 542 119.5 ± 128.6 pptv. The NO₃ production rate was comparable to that in urban areas such as
 543 north China and the Yangtze River Delta, with an average value of 1.5 ± 0.9 ppbv h⁻¹ and
 544 maximum of up to 5.84 ppbv h⁻¹, indicating an active nighttime chemical process in that
 545 area.



546 Further analysis of N_2O_5 and NO_3 steady state lifetimes indicates that NO_3 had a very short
547 average life of 0.5 ± 0.6 minutes, which was to some extent comparable to that in urban
548 areas in summer. The combination of the high NO_3 production rate and short lifetime
549 suggests a rapid NO_3 loss at night. While N_2O_5 uptake is inefficient in relatively clean air
550 masses. The nighttime $k(\text{NO}_3)$ corresponded to a NO_3 lifetime of 4.5 minutes, indicating
551 that VOCs also contribute little to NO_3 loss. Both VOC and N_2O_5 uptake can only explain
552 less than 20% of the loss. The fast NO_3 loss rate also indicated the less aged air mass that
553 was influenced by surface-level emissions. We infer that the local weak NO emission may
554 significantly change the near-surface chemical pattern of NO_3 chemistry, which may result
555 in a huge difference between the observed results on the island and those on the sea surface.
556 We suggested that future field measurements should be made on sea surfaces away from
557 islands, such as ship cruise observation, to get a comprehensive understanding of the
558 nocturnal NO_3 chemistry in the background marine regions.

559

560 **Code/Data availability.** The datasets used in this study are available at:
561 <https://doi.org/10.5281/zenodo.8089100> (Wang et al., 2023).

562 **Author contributions.** H.C.W. and Y. J.T. designed the study. J.W. and H.C.W. analyzed
563 the data with input from H.J.H., Z.L.Z., G.Z.F., C.Z.S., Z.H.L., J.Z., S.J.F. H.C.W., L.M.
564 Y. J.T., Z.H.L., and J.Z. organized this field campaign and provided the field measurement
565 dataset. J.W., H.C.W., and Y.J.T. wrote the paper. All authors commented on and edited the
566 manuscript.

567 **Acknowledgments**

568 This work was supported by the National Natural Science Foundation of China (Nos.
569 42175111), the Guangdong Major Project of Basic and Applied Basic Research (No.
570 2020B0301030004), Guangdong Basic and Applied Basic Research Foundation
571 (2022A1515010852), and the Fundamental Research Funds for the Central Universities,
572 Sun Yat-sen University (23lgbj002, 23hytd002). L.M. acknowledges the Zhuhai Science
573 and Technology Plan Project (ZH22036201210115PWC).

574

575 **Competing interests.** The authors declare that they have no conflicts of interest.

576

577 **Appendix A Supplementary data**

578 Supplementary data associated with this article can be found in the online version at xxxxxx.

579

580 **Reference**

581 Aldener, M., Brown, S. S., Stark, H., Williams, E. J., Lerner, B. M., Kuster, W. C., Goldan,



- 582 P. D., Quinn, P. K., Bates, T. S., Fehsenfeld, F. C., and Ravishankara, A. R.: Reactivity
583 and loss mechanisms of NO₃ and N₂O₅ in a polluted marine environment: Results
584 from in situ measurements during New England Air Quality Study 2002, *Journal of*
585 *Geophysical Research-Atmospheres*, 111, Artn D23s73, Doi 10.1029/2006jd007252,
586 2006.
- 587 Allan, B. J., Carslaw, N., Coe, H., Burgess, R. A., and Plane, J. M. C.: Observations of the
588 nitrate radical in the marine boundary layer, *Journal of Atmospheric Chemistry*, 33,
589 129-154, Doi 10.1023/A:1005917203307, 1999.
- 590 Atkinson, R., Baulch, D. L., Cox, R. A., Crowley, J. N., Hampson, R. F., Hynes, R. G.,
591 Jenkin, M. E., Rossi, M. J., and Troe, J.: Evaluated kinetic and photochemical data for
592 atmospheric chemistry: Volume I - gas phase reactions of O-x, HO_x, NO_x and SO_x
593 species, *Atmospheric Chemistry and Physics*, 4, 1461-1738, DOI 10.5194/acp-4-
594 1461-2004, 2004.
- 595 Ayres, B. R., Allen, H. M., Draper, D. C., Brown, S. S., Wild, R. J., Jimenez, J. L., Day, D.
596 A., Campuzano-Jost, P., Hu, W., de Gouw, J., Koss, A., Cohen, R. C., Duffey, K. C.,
597 Romer, P., Baumann, K., Edgerton, E., Takahama, S., Thornton, J. A., Lee, B. H.,
598 Lopez-Hilfiker, F. D., Mohr, C., Wennberg, P. O., Nguyen, T. B., Teng, A., Goldstein,
599 A. H., Olson, K., and Fry, J. L.: Organic nitrate aerosol formation via NO₃ + biogenic
600 volatile organic compounds in the southeastern United States, *Atmospheric Chemistry*
601 *and Physics*, 15, 13377-13392, 10.5194/acp-15-13377-2015, 2015.
- 602 Behnke, W., and V., Scheer, and, C., and Zetzsch: 16 O₄ Formation of ClNO₂ and HNO₃
603 in the presence of N₂O₅ and wet pure NaCl- and wet mixed NaCl/Na₂SO₄- aerosol,
604 *J Aerosol Sci*, 24, S115-S116, 1993.
- 605 Belloli, R., Barletta, B., Bolzacchini, E., and Meinardi, S.: Determination of toxic
606 nitrophenols in the atmosphere by high-performance liquid chromatography, *Journal*
607 *of Chromatography A*, 1999.
- 608 Bertram, T. H. and Thornton, J. A.: Toward a general parameterization of N₂O₅ reactivity
609 on aqueous particles: the competing effects of particle liquid water, nitrate and
610 chloride, *Atmospheric Chemistry and Physics*, 9, 8351-8363, 2009.
- 611 Brown, S. S. and Stutz, J.: Nighttime radical observations and chemistry, *Chem Soc Rev*,
612 41, 6405-6447, Doi 10.1039/C2cs35181a, 2012.
- 613 Brown, S. S., Stark, H., and Ravishankara, A. R.: Applicability of the steady state
614 approximation to the interpretation of atmospheric observations of NO₃ and N₂O₅,
615 *Journal of Geophysical Research-Atmospheres*, 108, Artn 4539, Doi
616 10.1029/2003jd003407, 2003.
- 617 Brown, S. S., Dube, W. P., Tham, Y. J., Zha, Q. Z., Xue, L. K., Poon, S., Wang, Z., Blake,
618 D. R., Tsui, W., Parrish, D. D., and Wang, T.: Nighttime chemistry at a high altitude
619 site above Hong Kong, *Journal of Geophysical Research-Atmospheres*, 121, 2457-
620 2475, 10.1002/2015jd024566, 2016.



- 621 Brown, S. S., Ryerson, T. B., Wollny, A. G., Brock, C. A., Peltier, R., Sullivan, A. P., Weber,
622 R. J., Dube, W. P., Trainer, M., Meagher, J. F., Fehsenfeld, F. C., and Ravishankara, A.
623 R.: Variability in nocturnal nitrogen oxide processing and its role in regional air quality,
624 Science, 311, 67-70, DOI 10.1126/science.1120120, 2006.
- 625 Brown, S. S., Dube, W. P., Peischl, J., Ryerson, T. B., Atlas, E., Warneke, C., de Gouw, J.
626 A., Hekkert, S. T., Brock, C. A., Flocke, F., Trainer, M., Parrish, D. D., Fehsenfeld, F.
627 C., and Ravishankara, A. R.: Budgets for nocturnal VOC oxidation by nitrate radicals
628 aloft during the 2006 Texas Air Quality Study, Journal of Geophysical Research-
629 Atmospheres, 116, Artn D24305, 10.1029/2011jd016544, 2011.
- 630 Brown, S. S., Dube, W. P., Fuchs, H., Ryerson, T. B., Wollny, A. G., Brock, C. A., Bahreini,
631 R., Middlebrook, A. M., Neuman, J. A., Atlas, E., Roberts, J. M., Osthoff, H. D.,
632 Trainer, M., Fehsenfeld, F. C., and Ravishankara, A. R.: Reactive uptake coefficients
633 for N₂O₅ determined from aircraft measurements during the Second Texas Air
634 Quality Study: Comparison to current model parameterizations, Journal of
635 Geophysical Research-Atmospheres, 114, Artn D00f10, 10.1029/2008jd011679, 2009.
- 636 Brown, S. S., Dube, W. P., Osthoff, H. D., Stutz, J., Ryerson, T. B., Wollny, A. G., Brock,
637 C. A., Warneke, C., De Gouw, J. A., Atlas, E., Neuman, J. A., Holloway, J. S., Lerner,
638 B. M., Williams, E. J., Kuster, W. C., Goldan, P. D., Angevine, W. M., Trainer, M.,
639 Fehsenfeld, F. C., and Ravishankara, A. R.: Vertical profiles in NO₃ and N₂O₅
640 measured from an aircraft: Results from the NOAA P-3 and surface platforms during
641 the New England Air Quality Study 2004, Journal of Geophysical Research-
642 Atmospheres, 112, Artn D22304, 10.1029/2007jd008883, 2007.
- 643 Brown, S. S., Dibb, J. E., Stark, H., Aldener, M., Vozella, M., Whitlow, S., Williams, E. J.,
644 Lerner, B. M., Jakoubek, R., Middlebrook, A. M., DeGouw, J. A., Warneke, C.,
645 Goldan, P. D., Kuster, W. C., Angevine, W. M., Sueper, D. T., Quinn, P. K., Bates, T.
646 S., Meagher, J. F., Fehsenfeld, F. C., and Ravishankara, A. R.: Nighttime removal of
647 NO_x in the summer marine boundary layer, Geophysical Research Letters, 31, Artn
648 L07108, Doi 10.1029/2004gl019412, 2004.
- 649 Chen, X., Wang, H., and Lu, K.: Interpretation of NO₃-
650 N₂O₅ observation via steady state
651 in high-aerosol air mass: the impact of equilibrium coefficient in ambient conditions,
652 Atmospheric Chemistry and Physics, 22, 3525-3533, 10.5194/acp-22-3525-2022,
653 2022.
- 654 Chuang, M.-T., Chang, S.-C., Lin, N.-H., Wang, J.-L., Sheu, G.-R., Chang, Y.-J., and Lee,
655 C.-T.: Aerosol chemical properties and related pollutants measured in Dongsha Island
656 in the northern South China Sea during 7-SEAS/Dongsha Experiment, Atmospheric
657 Environment, 78, 82-92, 10.1016/j.atmosenv.2012.05.014, 2013.
- 658 Crowley, J. N., Thieser, J., Tang, M. J., Schuster, G., Bozem, H., Beygi, Z. H., Fischer, H.,
659 Diesch, J. M., Drewnick, F., Borrmann, S., Song, W., Yassaa, N., Williams, J., Pöhler,



- 660 D., Platt, U., and Lelieveld, J.: Variable lifetimes and loss mechanisms for NO₃ and
661 N₂O₅ during the DOMINO campaign: contrasts between marine, urban and
662 continental air, *Atmospheric Chemistry and Physics*, 11, 10853-10870, 10.5194/acp-
663 11-10853-2011, 2011.
- 664 Delhomme, O., Morville, S., and Millet, M.: Seasonal and diurnal variations of atmospheric
665 concentrations of phenols and nitrophenols measured in the Strasbourg area, France,
666 *Atmospheric Pollution Research*, 1, 16-22, 10.5094/apr.2010.003, 2010.
- 667 Dewald, P., Nussbaumer, C. M., Schuladen, J., Ringsdorf, A., Edtbauer, A., Fischer, H.,
668 Williams, J., Lelieveld, J., and Crowley, J. N.: Fate of the nitrate radical at the summit
669 of a semi-rural mountain site in Germany assessed with direct reactivity
670 measurements, *Atmospheric Chemistry and Physics*, 22, 7051-7069, 10.5194/acp-22-
671 7051-2022, 2022.
- 672 Edwards, P. M., Aikin, K. C., Dube, W. P., Fry, J. L., Gilman, J. B., de Gouw, J. A., Graus,
673 M. G., Hanisco, T. F., Holloway, J., Huber, G., Kaiser, J., Keutsch, F. N., Lerner, B.
674 M., Neuman, J. A., Parrish, D. D., Peischl, J., Pollack, I. B., Ravishankara, A. R.,
675 Roberts, J. M., Ryerson, T. B., Trainer, M., Veres, P. R., Wolfe, G. M., Warneke, C.,
676 and Brown, S. S.: Transition from high- to low-NO_x control of night-time oxidation
677 in the southeastern US, *Nat Geosci*, 10, 490-+, 10.1038/Ngeo2976, 2017.
- 678 Evans, M. J. and Jacob, D. J.: Impact of new laboratory studies of N₂O₅ hydrolysis on
679 global model budgets of tropospheric nitrogen oxides, ozone, and OH, *Geophysical*
680 *Research Letters*, 32, Artn L09813, Doi 10.1029/2005gl022469, 2005.
- 681 Fuentes., J. D., Lerdau., M., and Atkinson., R.: Biogenic hydrocarbons in the atmospheric
682 Boundary A review, *B Am Meteorol Soc*, 2000.
- 683 Geyer, A., Alicke, B., Konrad, S., Schmitz, T., Stutz, J., and Platt, U.: Chemistry and
684 oxidation capacity of the nitrate radical in the continental boundary layer near Berlin,
685 *Journal of Geophysical Research-Atmospheres*, 106, 8013-8025, Doi
686 10.1029/2000jd900681, 2001.
- 687 Hallquist, M., Stewart, D. J., Stephenson, S. K., and Cox, R. A.: Hydrolysis of N₂O₅ on
688 sub-micron sulfate aerosols, *Phys Chem Chem Phys*, 5, 3453-3463, Doi
689 10.1039/B301827j, 2003.
- 690 Ian Barnes, Jens Hjorth, and Mihalopoulos, N.: Dimethyl Sulfide and Dimethyl Sulfoxide
691 and Their Oxidation in the Atmosphere, *Chem Rev*, 2006.
- 692 Kane, S. M., Caloz, F., and Leu, M. T.: Heterogeneous uptake of gaseous N₂O₅ by
693 (NH₄)₂SO₄, NH₄HSO₄, and H₂SO₄ aerosols, *J Phys Chem A*, 105, 6465-6470,
694 Doi 10.1021/Jp010490x, 2001.
- 695 Kiendler-Scharr, A., Mensah, A. A., Friese, E., Topping, D., Nemitz, E., Prevot, A. S. H.,
696 Aijala, M., Allan, J., Canonaco, F., Canagaratna, M., Carbone, S., Crippa, M., Dall
697 Osto, M., Day, D. A., De Carlo, P., Di Marco, C. F., Elbern, H., Eriksson, A., Freney,
698 E., Hao, L., Herrmann, H., Hildebrandt, L., Hillamo, R., Jimenez, J. L., Laaksonen,



- 699 A., McFiggans, G., Mohr, C., O'Dowd, C., Otjes, R., Ovadnevaite, J., Pandis, S. N.,
700 Poulain, L., Schlag, P., Sellegri, K., Swietlicki, E., Tiitta, P., Vermeulen, A., Wahner,
701 A., Worsnop, D., and Wu, H. C.: Ubiquity of organic nitrates from nighttime chemistry
702 in the European submicron aerosol, *Geophysical Research Letters*, 43, 7735-7744,
703 10.1002/2016gl069239, 2016.
- 704 Li, Z., Xie, P., Hu, R., Wang, D., Jin, H., Chen, H., Lin, C., and Liu, W.: Observations of
705 N₂O₅ and NO₃ at a suburban environment in Yangtze river delta in China: Estimating
706 heterogeneous N₂O₅ uptake coefficients, *J Environ Sci (China)*, 95, 248-255,
707 10.1016/j.jes.2020.04.041, 2020.
- 708 Liebmann, J., Karu, E., Sobanski, N., Schuladen, J., Ehn, M., Schallhart, S., Quelever, L.,
709 Hellen, H., Hakola, H., Hoffmann, T., Williams, J., Fischer, H., Lelieveld, J., and
710 Crowley, J. N.: Direct measurement of NO₃ radical reactivity in a boreal forest,
711 *Atmospheric Chemistry and Physics*, 18, 3799-3815, 10.5194/acp-18-3799-2018,
712 2018a.
- 713 Liebmann, J. M., Muller, J. B. A., Kubistin, D., Claude, A., Holla, R., Plass-Dulmer, C.,
714 Lelieveld, J., and Crowley, J. N.: Direct measurements of NO₃ reactivity in and above
715 the boundary layer of a mountaintop site: identification of reactive trace gases and
716 comparison with OH reactivity, *Atmospheric Chemistry and Physics*, 18, 12045-
717 12059, 10.5194/acp-18-12045-2018, 2018b.
- 718 Lin, C., Hu, R., Xie, P., Lou, S., Zhang, G., Tong, J., Liu, J., and Liu, W.: Nocturnal
719 atmospheric chemistry of NO₃ and N₂O₅ over Changzhou in the Yangtze River Delta
720 in China, *J Environ Sci (China)*, 114, 376-390, 10.1016/j.jes.2021.09.016, 2022.
- 721 Liu, X., Lyu, X., Wang, Y., Jiang, F., and Guo, H.: Intercomparison of
722 O₃ formation and radical chemistry in the past decade at a
723 suburban site in Hong Kong, *Atmospheric Chemistry and Physics*, 19, 5127-5145,
724 10.5194/acp-19-5127-2019, 2019.
- 725 Liu, X. G., Gu, J. W., Li, Y. P., Cheng, Y. F., Qu, Y., Han, T. T., Wang, J. L., Tian, H. Z.,
726 Chen, J., and Zhang, Y. H.: Increase of aerosol scattering by hygroscopic growth:
727 Observation, modeling, and implications on visibility, *Atmospheric Research*, 132,
728 91-101, 10.1016/j.atmosres.2013.04.007, 2013.
- 729 Lu, X., Qin, M., Xie, P., Duan, J., Fang, W., and Liu, W.: Observation of ambient NO(3)
730 radicals by LP-DOAS at a rural site in North China Plain, *Sci Total Environ*, 804,
731 149680, 10.1016/j.scitotenv.2021.149680, 2022.
- 732 Mogensen, D., Gierens, R., Crowley, J. N., Keronen, P., Smolander, S., Sogachev, A.,
733 Nolscher, A. C., Zhou, L., Kulmala, M., Tang, M. J., Williams, J., and Boy, M.:
734 Simulations of atmospheric OH, O₃ and NO₃ reactivities within and above the boreal
735 forest, *Atmospheric Chemistry and Physics*, 15, 3909-3932, 10.5194/acp-15-3909-
736 2015, 2015.
- 737 Morgan, W. T., Ouyang, B., Allan, J. D., Aruffo, E., Di Carlo, P., Kennedy, O. J., Lowe, D.,



- 738 Flynn, M. J., Rosenberg, P. D., Williams, P. I., Jones, R., McFiggans, G. B., and Coe,
739 H.: Influence of aerosol chemical composition on N₂O₅ uptake: airborne regional
740 measurements in northwestern Europe, *Atmospheric Chemistry and Physics*, 15, 973-
741 990, DOI 10.5194/acp-15-973-2015, 2015.
- 742 Ng, N. L., Brown, S. S., Archibald, A. T., Atlas, E., Cohen, R. C., Crowley, J. N., Day, D.
743 A., Donahue, N. M., Fry, J. L., Fuchs, H., Griffin, R. J., Guzman, M. I., Herrmann, H.,
744 Hodzic, A., Iinuma, Y., Jimenez, J. L., Kiendler-Scharr, A., Lee, B. H., Luecken, D. J.,
745 Mao, J. Q., McLaren, R., Mutzel, A., Osthoff, H. D., Ouyang, B., Picquet-Varrault, B.,
746 Platt, U., Pye, H. O. T., Rudich, Y., Schwantes, R. H., Shiraiwa, M., Stutz, J., Thornton,
747 J. A., Tilgner, A., Williams, B. J., and Zaveri, R. A.: Nitrate radicals and biogenic
748 volatile organic compounds: oxidation, mechanisms, and organic aerosol,
749 *Atmospheric Chemistry and Physics*, 17, 2103-2162, 10.5194/acp-17-2103-2017,
750 2017.
- 751 Niu, Y. B., Zhu, B., He, L. Y., Wang, Z., Lin, X. Y., Tang, M. X., and Huang, X. F.: Fast
752 Nocturnal Heterogeneous Chemistry in a Coastal Background Atmosphere and Its
753 Implications for Daytime Photochemistry, *Journal of Geophysical Research:*
754 *Atmospheres*, 127, 10.1029/2022jd036716, 2022.
- 755 Osthoff, H. D., Pilling, M. J., Ravishankara, A. R., and Brown, S. S.: Temperature
756 dependence of the NO(3) absorption cross-section above 298 K and determination of
757 the equilibrium constant for NO(3)+NO(2) <-> N(2)O(5) at atmospherically relevant
758 conditions, *Phys Chem Chem Phys*, 9, 5785-5793, 10.1039/b709193a, 2007.
- 759 Osthoff, H. D., Roberts, J. M., Ravishankara, A. R., Williams, E. J., Lerner, B. M.,
760 Sommariva, R., Bates, T. S., Coffman, D., Quinn, P. K., Dibb, J. E., Stark, H.,
761 Burkholder, J. B., Talukdar, R. K., Meagher, J., Fehsenfeld, F. C., and Brown, S. S.:
762 High levels of nitryl chloride in the polluted subtropical marine boundary layer, *Nat*
763 *Geosci*, 1, 324-328, Doi 10.1038/Ngeo177, 2008.
- 764 Riedel, T. P., Bertram, T. H., Crisp, T. A., Williams, E. J., Lerner, B. M., Vlasenko, A., Li,
765 S. M., Gilman, J., de Gouw, J., Bon, D. M., Wagner, N. L., Brown, S. S., and Thornton,
766 J. A.: Nitryl Chloride and Molecular Chlorine in the Coastal Marine Boundary Layer,
767 *Environmental Science & Technology*, 46, 10463-10470, 10.1021/es204632r, 2012.
- 768 Riedel, T. P., Wolfe, G. M., Danas, K. T., Gilman, J. B., Kuster, W. C., Bon, D. M., Vlasenko,
769 A., Li, S. M., Williams, E. J., Lerner, B. M., Veres, P. R., Roberts, J. M., Holloway, J.
770 S., Lefer, B., Brown, S. S., and Thornton, J. A.: An MCM modeling study of nitryl
771 chloride (ClNO₂) impacts on oxidation, ozone production and nitrogen oxide
772 partitioning in polluted continental outflow, *Atmospheric Chemistry and Physics*, 14,
773 3789-3800, 10.5194/acp-14-3789-2014, 2014.
- 774 Rosati, B., Isokääntä, S., Christiansen, S., Jensen, M. M., Moosakutty, S. P., Wollesen de
775 Jonge, R., Massling, A., Glasius, M., Elm, J., Virtanen, A., and Bilde, M.:
776 Hygroscopicity and CCN potential of DMS-derived aerosol particles, *Atmospheric*



- 777 Chemistry and Physics, 22, 13449-13466, 10.5194/acp-22-13449-2022, 2022.
- 778 Tang, M. J., Schuster, G., and Crowley, J. N.: Heterogeneous reaction of N₂O₅ with illite
779 and Arizona test dust particles, *Atmospheric Chemistry and Physics*, 14, 245-254,
780 DOI 10.5194/acp-14-245-2014, 2014.
- 781 Tham, Y. J., Wang, Z., Li, Q. Y., Wang, W. H., Wang, X. F., Lu, K. D., Ma, N., Yan, C.,
782 Kecorius, S., Wiedensohler, A., Zhang, Y. H., and Wang, T.: Heterogeneous N₂O₅
783 uptake coefficient and production yield of ClNO₂ in polluted northern China: roles of
784 aerosol water content and chemical composition, *Atmospheric Chemistry and Physics*,
785 18, 13155-13171, 10.5194/acp-18-13155-2018, 2018.
- 786 Tham, Y. J., Wang, Z., Li, Q. Y., Yun, H., Wang, W. H., Wang, X. F., Xue, L. K., Lu, K. D.,
787 Ma, N., Bohn, B., Li, X., Kecorius, S., Gross, J., Shao, M., Wiedensohler, A., Zhang,
788 Y. H., and Wang, T.: Significant concentrations of nitryl chloride sustained in the
789 morning: investigations of the causes and impacts on ozone production in a polluted
790 region of northern China, *Atmospheric Chemistry and Physics*, 16, 14959-14977,
791 10.5194/acp-16-14959-2016, 2016.
- 792 Thornton, J. A., Kercher, J. P., Rie De L, T. P., Wagner, N. L., Cozic, J., Holloway, J. S.,
793 Dubé, W., Wolfe, G. M., Quinn, P. K., and Middlebrook, A. M.: A large atomic
794 chlorine source inferred from mid-continental reactive nitrogen chemistry, *Nature*,
795 464, 271-274, 2010.
- 796 Vrekoussis, M., Mihalopoulos, N., Gerasopoulos, E., Kanakidou, M., Crutzen, P. J., and
797 Lelieveld, J.: Two-years of NO₃ radical observations in the boundary layer over the
798 Eastern Mediterranean, *Atmospheric Chemistry and Physics*, 7, 315-327, 2007.
- 799 Vrekoussis, M., Kanakidou, M., Mihalopoulos, N., Crutzen, P. J., Lelieveld, J., Perner, D.,
800 Berresheim, H., and Baboukas, E.: Role of the NO₃ radicals in oxidation processes in
801 the eastern Mediterranean troposphere during the MINOS campaign, *Atmospheric
802 Chemistry and Physics*, 4, 169-182, 2004.
- 803 Wagner, N. L., Riedel, T. P., Young, C. J., Bahreini, R., Brock, C. A., Dube, W. P., Kim, S.,
804 Middlebrook, A. M., Ozturk, F., Roberts, J. M., Russo, R., Sive, B., Swarthout, R.,
805 Thornton, J. A., VandenBoer, T. C., Zhou, Y., and Brown, S. S.: N₂O₅ uptake
806 coefficients and nocturnal NO₂ removal rates determined from ambient wintertime
807 measurements, *Journal of Geophysical Research-Atmospheres*, 118, 9331-9350, Doi
808 10.1002/Jgrd.50653, 2013.
- 809 Wang, H., Chen, J., and Lu, K.: Development of a portable cavity-enhanced absorption
810 spectrometer for the measurement of ambient NO₃ and N₂O₅: experimental setup,
811 lab characterizations, and field applications in a polluted urban environment, *Atmos
812 Meas Tech*, 10, 1465-1479, 10.5194/amt-10-1465-2017, 2017a.
- 813 Wang, H., Chen, T., and Lu, K.: Measurement of NO₃ and N₂O₅ in the Troposphere,
814 *Progress in Chemistry*, 27, 963-976, 10.7536/pc141230, 2015.
- 815 Wang, H., Lu, K., Chen, S., Li, X., Zeng, L., Hu, M., and Zhang, Y.: Characterizing nitrate



- 816 radical budget trends in Beijing during 2013–2019, *Science of The Total Environment*,
817 795, 10.1016/j.scitotenv.2021.148869, 2021.
- 818 Wang, H., Wang, H., Lu, X., Lu, K., Zhang, L., Tham, Y. J., Shi, Z., Aikin, K., Fan, S.,
819 Brown, S. S., and Zhang, Y.: Increased night-time oxidation over China despite
820 widespread decrease across the globe, *Nat Geosci*, 10.1038/s41561-022-01122-x,
821 2023.
- 822 Wang, H., Lyu, X., Guo, H., Wang, Y., Zou, S., Ling, Z., Wang, X., Jiang, F., Zeren, Y., Pan,
823 W., Huang, X., and Shen, J.: WS-Ozone pollution around a coastal region of South
824 China Sea: interaction between marine and continental air, *Atmospheric Chemistry
825 and Physics*, 18, 4277-4295, 10.5194/acp-18-4277-2018, 2018a.
- 826 Wang, H., Chen, X., Lu, K., Hu, R., Li, Z., Wang, H., Ma, X., Yang, X., Chen, S., Dong,
827 H., Liu, Y., Fang, X., Zeng, L., Hu, M., and Zhang, Y.: NO₃ and N₂O₅ chemistry at a
828 suburban site during the EXPLORE-YRD campaign in 2018, *Atmospheric
829 Environment*, 224, 10.1016/j.atmosenv.2019.117180, 2020a.
- 830 Wang, H., Chen, X., Lu, K., Tan, Z., Ma, X., Wu, Z., Li, X., Liu, Y., Shang, D., Wu, Y.,
831 Zeng, L., Hu, M., Schmitt, S., Kiendler-Scharr, A., Wahner, A., and Zhang, Y.:
832 Wintertime N₂O₅ uptake coefficients over the North China Plain, *Science Bulletin*,
833 65, 765-774, 10.1016/j.scib.2020.02.006, 2020b.
- 834 Wang, H., Lu, K., Guo, S., Wu, Z., Shang, D., Tan, Z., Wang, Y., Le Breton, M., Lou, S.,
835 Tang, M., Wu, Y., Zhu, W., Zheng, J., Zeng, L., Hallquist, M., Hu, M., and Zhang, Y.:
836 Efficient N₂O₅ uptake and NO₃ oxidation in the outflow of urban Beijing,
837 *Atmospheric Chemistry and Physics*, 18, 9705-9721, 10.5194/acp-18-9705-2018,
838 2018b.
- 839 Wang, H., Lu, K., Chen, X., Zhu, Q., Chen, Q., Guo, S., Jiang, M., Li, X., Shang, D., Tan,
840 Z., Wu, Y., Wu, Z., Zou, Q., Zheng, Y., Zeng, L., Zhu, T., Hu, M., and Zhang, Y.: High
841 N₂O₅ Concentrations Observed in Urban Beijing: Implications of a Large Nitrate
842 Formation Pathway, *Environmental Science & Technology Letters*, 4, 416-420,
843 10.1021/acs.estlett.7b00341, 2017b.
- 844 Wang, H., Yuan, B., Zheng, E., Zhang, X., Wang, J., Lu, K., Ye, C., Yang, L., Huang, S.,
845 Hu, W., Yang, S., Peng, Y., Qi, J., Wang, S., He, X., Chen, Y., Li, T., Wang, W.,
846 Huangfu, Y., Li, X., Cai, M., Wang, X., and Shao, M.: Formation and impacts of nitryl
847 chloride in Pearl River Delta, *Atmospheric Chemistry and Physics*, 22, 14837-14858,
848 10.5194/acp-22-14837-2022, 2022.
- 849 Wang, S. S., Shi, C. Z., Zhou, B., Zhao, H., Wang, Z. R., Yang, S. N., and Chen, L. M.:
850 Observation of NO₃ radicals over Shanghai, China, *Atmospheric Environment*, 70,
851 401-409, DOI 10.1016/j.atmosenv.2013.01.022, 2013.
- 852 Wang, X. F., Wang, H., Xue, L. K., Wang, T., Wang, L. W., Gu, R. R., Wang, W. H., Tham,
853 Y. J., Wang, Z., Yang, L. X., Chen, J. M., and Wang, W. X.: Observations of N₂O₅
854 and ClNO₂ at a polluted urban surface site in North China: High N₂O₅ uptake



- 855 coefficients and low ClNO₂ product yields, *Atmospheric Environment*, 156, 125-134,
856 10.1016/j.atmosenv.2017.02.035, 2017c.
- 857 Wang, Z., Wang, W. H., Tham, Y. J., Li, Q. Y., Wang, H., Wen, L., Wang, X. F., and Wang,
858 T.: Fast heterogeneous N₂O₅ uptake and ClNO₂ production in power plant and
859 industrial plumes observed in the nocturnal residual layer over the North China Plain,
860 *Atmospheric Chemistry and Physics*, 17, 12361-12378, 10.5194/acp-17-12361-2017,
861 2017d.
- 862 Wang, J., Wang, H., Tham, Y. J., Ming, L., Zheng, Z., Fang, G., Sun, C., Ling, Z., Zhao, J.,
863 and Fan, S.. (2023). Measurement report: Atmospheric nitrate radical chemistry in the
864 South China Sea influenced by the urban outflow of the Pearl River Delta [Data set].
865 Zenodo. <https://doi.org/10.5281/zenodo.8089100>.
- 866 Warneke, C., de Gouw, J. A., Goldan, P. D., Kuster, W. C., Williams, E. J., Lerner, B. M.,
867 Jakoubek, R., Brown, S. S., Stark, H., Aldener, M., Ravishankara, A. R., Roberts, J.
868 M., Marchewka, M., Bertman, S., Sueper, D. T., McKeen, S. A., Meagher, J. F., and
869 Fehsenfeld, F. C.: Comparison of daytime and nighttime oxidation of biogenic and
870 anthropogenic VOCs along the New England coast in summer during New England
871 Air Quality Study 2002, *Journal of Geophysical Research-Atmospheres*, 109, Art
872 D10309, 10.1029/2003jd004424, 2004.
- 873 Wayne, R. P., Barnes, I., Biggs, P., Burrows, J. P., Canosamas, C. E., Hjorth, J., Lebras, G.,
874 Moortgat, G. K., Perner, D., Poulet, G., Restelli, G., and Sidebottom, H.: The Nitrate
875 Radical - Physics, Chemistry, and the Atmosphere, *Atmos Environ a-Gen*, 25, 1-203,
876 Doi 10.1016/0960-1686(91)90192-A, 1991.
- 877 Wood, E. C., Bertram, T. H., Wooldridge, P. J., and Cohen, R. C.: Measurements of N₂O₅,
878 NO₂, and O₃ east of the San Francisco Bay, 2005.
- 879 Xu, L., Guo, H., Boyd, C. M., Klein, M., Bougiatioti, A., Cerully, K. M., Hite, J. R.,
880 Isaacman-VanWertz, G., Kreisberg, N. M., Knote, C., Olson, K., Koss, A., Goldstein,
881 A. H., Hering, S. V., de Gouw, J., Baumann, K., Lee, S. H., Nenes, A., Weber, R. J.,
882 and Ng, N. L.: Effects of anthropogenic emissions on aerosol formation from isoprene
883 and monoterpenes in the southeastern United States (vol 112, pg 37, 2015), *P Natl
884 Acad Sci USA*, 112, E4506-E4507, 2015.
- 885 Yan, C., Tham, Y. J., Zha, Q. Z., Wang, X. F., Xue, L. K., Dai, J. N., Wang, Z., and Wang,
886 T.: Fast heterogeneous loss of N₂O₅ leads to significant nighttime NO_x removal and
887 nitrate aerosol formation at a coastal background environment of southern China,
888 *Science of the Total Environment*, 677, 637-647, 10.1016/j.scitotenv.2019.04.389,
889 2019.
- 890 Yan, Y., Wang, S., Zhu, J., Guo, Y., Tang, G., Liu, B., An, X., Wang, Y., and Zhou, B.:
891 Vertically increased NO(3) radical in the nocturnal boundary layer, *Sci Total Environ*,
892 763, 142969, 10.1016/j.scitotenv.2020.142969, 2021.
- 893 Yang, S., Yuan, B., Peng, Y., Huang, S., Chen, W., Hu, W., Pei, C., Zhou, J., Parrish, D. D.,



- 894 Wang, W., He, X., Cheng, C., Li, X.-B., Yang, X., Song, Y., Wang, H., Qi, J., Wang,
895 B., Wang, C., Wang, C., Wang, Z., Li, T., Zheng, E., Wang, S., Wu, C., Cai, M., Ye,
896 C., Song, W., Cheng, P., Chen, D., Wang, X., Zhang, Z., Wang, X., Zheng, J., and Shao,
897 M.: The formation and mitigation of nitrate pollution: comparison between urban and
898 suburban environments, *Atmospheric Chemistry and Physics*, 22, 4539-4556,
899 10.5194/acp-22-4539-2022, 2022.
- 900 Yu, C., Wang, Z., Xia, M., Fu, X., Wang, W., Tham, Y. J., Chen, T., Zheng, P., Li, H., Shan,
901 Y., Wang, X., Xue, L., Zhou, Y., Yue, D., Ou, Y., Gao, J., Lu, K., Brown, S. S., Zhang,
902 Y., and Wang, T.: Heterogeneous N₂O₅ reactions on atmospheric aerosols at four
903 Chinese sites: improving model representation of uptake parameters, *Atmos. Chem.*
904 *Phys.*, 20, 4367-4378, 10.5194/acp-20-4367-2020, 2020.
- 905 Yun, H., Wang, T., Wang, W. H., Tham, Y. J., Li, Q. Y., Wang, Z., and Poon, S. C. N.:
906 Nighttime NO_x loss and ClNO₂ formation in the residual layer of a polluted region:
907 Insights from field measurements and an iterative box model, *Science of the Total*
908 *Environment*, 622, 727-734, 10.1016/j.scitotenv.2017.11.352, 2018a.
- 909 Yun, H., Wang, W. H., Wang, T., Xia, M., Yu, C., Wang, Z., Poon, S. C. N., Yue, D. L., and
910 Zhou, Y.: Nitrate formation from heterogeneous uptake of dinitrogen pentoxide during
911 a severe winter haze in southern China, *Atmospheric Chemistry and Physics*, 18,
912 17515-17527, 10.5194/acp-18-17515-2018, 2018b.
- 913 Zhou, W., Zhao, J., Ouyang, B., Mehra, A., Xu, W. Q., Wang, Y. Y., Bannan, T. J., Worrall,
914 S. D., Priestley, M., Bacak, A., Chen, Q., Xie, C. H., Wang, Q. Q., Wang, J. F., Du, W.,
915 Zhang, Y. J., Ge, X. L., Ye, P. L., Lee, J. D., Fu, P. Q., Wang, Z. F., Worsnop, D., Jones,
916 R., Percival, C. J., Coe, H., and Sun, Y. L.: Production of N₂O₅ and ClNO₂ in summer
917 in urban Beijing, China, *Atmospheric Chemistry and Physics*, 18, 11581-11597,
918 10.5194/acp-18-11581-2018, 2018.
- 919 Zhu, J., Newhook, R., Marro, L., and Chan, C. C.: Selected Volatile Organic Compounds
920 in Residential Air in the City of Ottawa, Canada, 2005.
- 921 Zhu, J., Wang, S., Zhang, S., Xue, R., Gu, C., and Zhou, B.: Changes in NO₃ adical and Its
922 Nocturnal Chemistry in Shanghai From 2014 to 2021 Revealed by Long - Term
923 Observation and a Stacking Model: Impact of China's Clean Air Action Plan, *Journal*
924 *of Geophysical Research: Atmospheres*, 127, 10.1029/2022jd037438, 2022.

925